LAPPEENRANTA UNIVERSITY OF TECHNOLOGY
LUT School of Energy Systems
LUT Mechanical Engineering

Ikechukwu Kingsley Chima

EXPERIMENTATION ON WIND POWERED HYDRAULIC HEATING SYSTEM

Examiners: Professor Heikki Handroos
D. Sc. (Tech.) Rafael Åman

ABSTRACT

Lappeenranta University of Technology
LUT School of Energy Systems
LUT Mechanical Engineering

Ikechukwu Kingsley Chima

Experimentation on wind powered hydraulic heating system

Master's thesis

2015

64 pages, 37 figures, 3 tables and 5 appendices

Examiners: Professor Heikki Handroos
D. Sc. (Mech. Eng.) Rafael Åman

Keywords: Savonius Rotor, Tip speed ratio, Torque coefficient, Fluid power circuit, Throttle valve, Optimum orifice diameter, Thermal power

It is common knowledge of the world's dependency on fossil fuel for energy, its unsustainability on the long run and the changing trend towards renewable energy as an alternative energy source. This aims to cut down greenhouse gas emission and its impact on the rate of ecological and climatic change. Quite remarkably, wind energy has been one of many focus areas of renewable energy sources and has attracted lots of investment and technological advancement. The objective of this research is to explore wind energy and its application in household heating. This research aims at applying experimental approach in real time to study and verify a virtually simulated wind powered hydraulic house heating system.

The hardware components comprise of an integrated hydraulic pump, flow control valve, hydraulic fluid and other hydraulic components. The system design and control applies hardware in-the-loop (HIL) simulation setup. Output signal from the semi-empirical turbine modelling controls the integrated motor to generate flow. Throttling the volume flow creates pressure drop across the valve and subsequently thermal power in the system to be outputted using a heat exchanger. Maximum thermal power is achieved by regulating valve orifice to achieve optimum system parameter.

Savonius rotor is preferred for its low inertia, high starting torque and ease of design and maintenance characteristics, but lags in power efficiency. A prototype turbine design is used; with power output in range of practical Savonius turbine. The physical mechanism of the prototype turbine's augmentation design is not known and will not be a focus in this study.

ACKNOWLEDGEMENTS

This master's thesis was carried out in the Laboratory of Intelligent Machines in Lappeenranta University of Technology during the 2014/2015 academic session.

My utmost appreciation goes to supervisors; Professor Handroos and D.Sc. (Tech.) Åman for their guidance and support through the different stages of this research. And not to forget to recognize the role of D.Sc. (Tech.) Lauri Luostarinen, and the laboratory personnel in the person of Mr. Juha Koivisto for their technical assistance.

The unweaning support of my family and close friends was of immense strength and deserves a heartfelt gratitude.

Ikechukwu Kingsley Chima
Lappeenranta 20.06.2015

TABLE OF CONTENTS

LIST OF SYMBOLS AND ABBREVIATIONS

A	Turbine cross-section area	[m^2]
A_o	Valve orifice area	[mm^2]
A_r	Radiative area	[m^2]
A_v	Poppet area normal to pressure	[m^2]
B	Intercept	
C_d	Discharge coefficient	
C_p	Turbine power coefficient	
C_{pk}	Valve power coefficient	
C_t	Turbine torque coefficient	
K_v	Flow coefficient	
C_{voil}	Specific heat capacity of oil	[J/kgK]
D	Diameter	[m]
E	Kinetic energy	[kg m^2/s^2]
F_c	Coulomb friction force	[N]
F_{s0}	Spring force preload	[N]
H	Height	[m]
h_t	Heat transfer coefficient	[W/m^{20}C]
J	Inertia	[kgm^2]
K	Gradient	
m	Mass of rotor	[kg]
m_w	Mass of wind	[kg]
M_p	Pump input torque	[Nm]
M_{wt}	Wind turbine output torque	[Nm]
p	System pressure	[Pa]
p_c	Cracking pressure	[Pa]
P_h	Heat load	[kW]
P_k	Thermal power	[W]

p_p	Pump pressure	[Pa]
P_r	Radiative power	[W]
P_{sc}	Specific cooling capacity	[kW/°C]
P_t	Tank power	[W]
P_v	Power loss	[kW]
P_w	Wind power	[W]
P_{wt}	Turbine power	[W]
Q	Volume flow	[m^3/s]
r	Radius	[m]
t	Time	[s]
T_1, T_2	Defined temperatures	[^{0}C]
T_f	Final oil temperature	[^{0}C]
T_t	Tank oil temperature	[^{0}C]
T_∞	Ambient oil temperature	[^{0}C]
T_a	Ambient air temperature	[^{0}C]
v	Wind velocity	[m/s]
V	Tank volume	[m^3]
V_k	Pump displacement	[m^3/rev]
X	Tip speed ratio value along x-axis	
$\dot{m}$	Mass flow rate	[kg/s]
$\ddot{\theta}$	Angular acceleration	[rad/s^2]
λ	Tip speed ratio	
ρ	Density of wind	[kg/m^3]
ρ_{oil}	Density of oil	[kg/ m^3]
ω	Angular velocity	[rad/s]
Δt	Time difference	[s]
Δp	Pressure difference	[Pa]

ADC	Analog to Digital Converter
DAC	Digital to Analog Converter

HAWT	Horizontal-Axis Wind Turbine
HIL	Hardware in-the-loop
IEHEC	Integrated Electro-Hydraulic Energy Converter
RTI	Real time interface

1 INTRODUCTION

This thesis work is based on virtually simulated hydraulic house heating model [1]. Via experimentation, a motor controlled to mimic a wind turbine is coupled to a novel hydraulic house heating system and utilized to study the energy conversion of wind energy into heat for house heating purpose. This approach of energy conversion to heat stems from the need to improve the efficiency of energy output and reduction of losses that accrue in wind to electrical energy conversion.

Savonius rotor is adopted as the test rotor for its low inertia, high starting torque in low wind, ease of design and maintenance characteristics. A prototype Savonius turbine model [2] was used and power achieved is in range of practical Savonius turbine power output. However no information about the physical mechanism of the turbine's augmentation design was made available by the source.

Wind has been one of many useful energy sources other applications other than power generation such as in grinding mills and irrigation purposes. The level of investment and technological development [3, 4, 5] in alternate power sources indicates an increasing interest over time in wind and other renewable energy applications for power generation. This is due to their sustainability, clean energy and availability for most part of the year. Wind energy is one of the key energy sources have providing alternative to fossil fuel but at a cost. To this end, technologies have been developed to harness this energy and more research is underway to optimize the efficiency of energy output from wind.

The idea of a compact and simple system design with Savonius rotor is aimed at solving the bulk nature of the widely used horizontal-axis wind turbine (HAWT). HAWT turbine hardware comprise of the following major components - rotor, nacelle (gearbox and generator), blades, tower and transformer [6, 7]. By adopting Savonius turbine, the system eliminates the need for a drivetrain, generator and heavy towers required to support HAWT turbine's weight while cutting down on costs incurred in power generation from wind energy.

The system design applies hardware in-the-loop (HIL) simulation setup. In HIL simulation, the virtually simulated system is operated in real-time with its simulated dynamic equivalent [8]. Application of HIL simulation is on the increase in model validation and testing by replacing parts of a simulation model of a system with hardware components. The flexibility HIL simulation offers in application to wide operating conditions improves reliability and better understanding of system interaction [9].

The turbine model is designed using mathematical equations of a typical Savonius rotor. The virtual turbine simulation integrated in the setup controls the output power of the electric motor connected in the setup. Signal response measured from hardware components are inputted into the simulation in real time.

The experimental set-up is an open-loop hydraulic circuit using an Integrated Electro-Hydraulic Energy Converter (IEHEC) as power source. The system comprises of an integrated electrical motor and a hydraulic pump, controlled using the inverter to mimic the dynamic behavior of wind turbine. The motor actuates the pump to produce the required volume flow in the system. Sets of valve; a pressure relief valve is mounted in the set-up to regulate pressure buildup as a safety measure. To constrict flow, a pin valve is used thereby generating heat in the hydraulic fluid. The heat generated is then outputted using a heat exchanger for useful house heating. The experimental result will be compared with the results of the virtually simulated turbine model [1] from earlier study.

The potential for this system is aimed for application in remote sites; hence easy of assembly and compactness are factors to consider in commercial design. Unlike in electrical power generation systems, access to the grid and frequency conversion mechanism are eliminated thereby avoiding need of transmission, high equipment costs and losses incurred. Direct heat conversion of wind energy is aimed at curtailing losses and improving the efficiency of wind energy conversion.

1.1 Background information

Application of hydraulic systems for energy generation is rather not a new field of study. As far back as June of 1977, a patent was registered of a system utilizing wind powered hydraulic heating system. This invention uses a wind velocity sensor and a valve control mechanism responsive to the sensor to control an adjustable pressure responsive relief valve which restricts the flow of hydraulic fluid thereby generating heat The sensor; a mechanical lever wind gauge coupled to the relief valve controls the valve opening with respect to the wind speed. Similar mechanism responsive to valve inlet pressure is utilized to close the valve with changing wind speed. [10]

A different experimental study [11] utilizing hydraulic throttling for domestic heating recorded an achieved room temperature heating up to 70 ^{0}C within 15 minutes. The outlined projects and many other researches in the field indicate growing interest in thermal energy generation using hydraulic system.

This project serves the purpose of studying thermal power generation from a hydraulic circuit driven by wind energy. Similar to the projects mentioned in [5] and [6], it differs in the source of the driving power and type of valve used. The optimum operating condition of the experimental systems will be noted. The experiment explores the virtual simulation guidelines. Results are to be corroborated and recommendation for improvement offered where possible. Calculated power values from the wind data is tabulated in the result section.

The systems' components comprise of a frequency converter controlled IEHEC motor which serves as the primary power source of the hydraulic circuit; mimicking the behavior of a wind rotor with defined operating parameter of a typical Savonius rotor subject to different wind speed. Other vital components of the hydraulic circuit are the flow control and pressure relief valves for flow constriction and regulation of system maximum set-point pressure respectively. At a set orifice area, oil flow is constricted creating pressure drop across the flow control valve. The heat generated is to be outputted to the surrounding using an oil-to-air cooler. Hydraulic tank and piping in the set-up serve the purpose of storing and transporting the hydraulic fluid. More so the tank would serve as a heat reservoir for the undissipated heat in the returning

hydraulic fluid. Tank capacity and heat loss to the environment are factor not accounted for in this study. Hence an ideal adiabatic and leakage free system set-up is considered.

It should be noted that of special interest in this research is the efficiency of performance of the throttle valve and parameters of the turbine and valve at which thermal power output is optimal. To demonstrate commercial application of the system, Fig. 1 shows the system's component assembly. It is worth noting that hydraulic house heating system is not limited to Savonius rotor, however in this study, Savonius rotor is the primary drive system harnessing the wind energy.

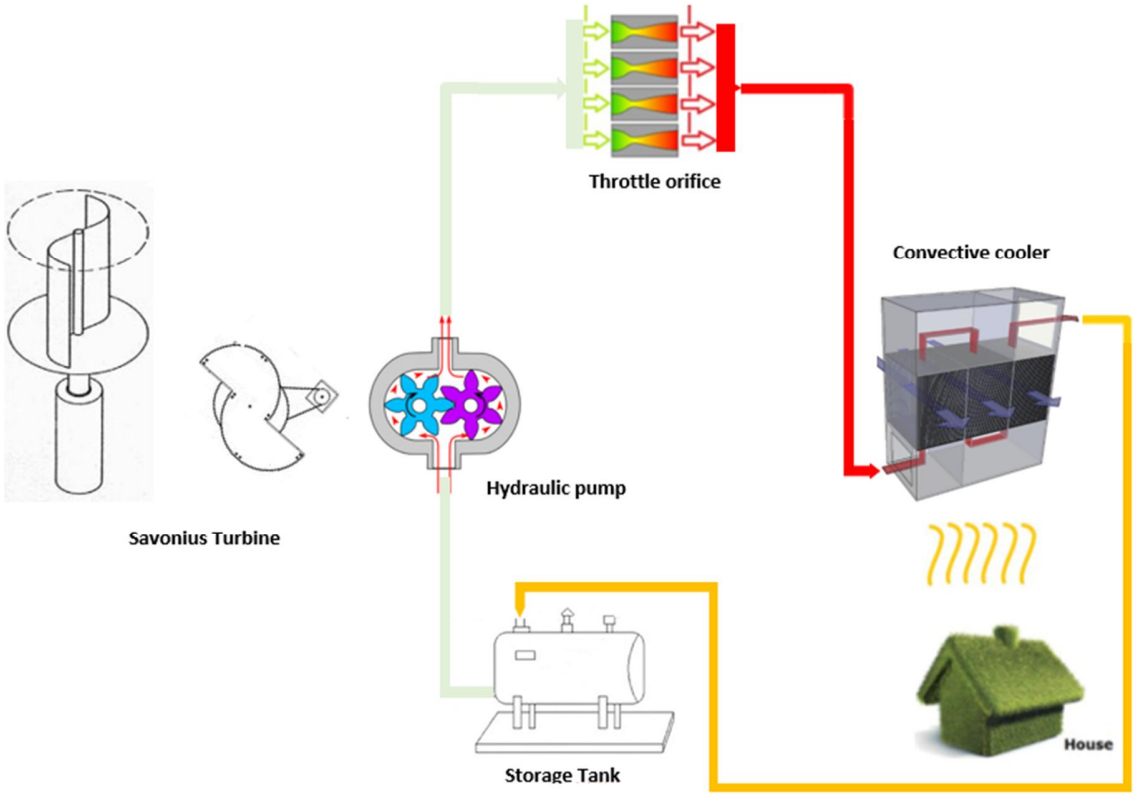

Figure 1. Schematic representation of system in commercial application.

1.2 Objectives and scope of research problem

The objective of this research work is to verify the results of the virtually simulated model using practical experiment and the possible commercialization of the system given a viable result from the experiment. Steps will be taken to improve the efficiency of thermal power generation by studying the behavior of the flow control valve (throttle valve) unit in more detail by comparing

the measured flow characteristics of the valve in the set-up with that provided by the manufacturer. The result is aimed at validating the semi-empirical approach applied in valve modelling in the experiment.

The valve in question is a needle valve which operates by manual adjustment to a desired set point. Going by the output result of the virtual simulation model, the maximum power is achieved when the orifice diameter was adjusted as such that the rotor tip speed ratio follows the power curve [1]. Hence a proportional valve could best be used to achieve this self-adjustment for operation at optimum tip speed ratio of the turbine. This will require to consider the energy requirement. However, use of proportional valve is beyond the scope of this research. In other words, an optimum valve orifice should be applied for the valve in use.

In the previous research, a measured wind speed was applied. This wind data was gathered by Finnish meteorological institute. The power output of the virtual turbine - and subsequently the thermal power output at average wind speed is in the range of 100-1000 W. For real-time simulation with the experimental set-up, a sample wind profile of constant wind speed (in range of 2 m/s to 12 m/s) over a time period was designed and used to study the system response.

The IEHEC motor offered a flexible and efficient substitute to the Savonius rotor. The parameters of a typical augmented Savonius rotor was used to harness the wind energy thereby driving the pump. More details of the rotor model and other physical components used in the system build-up will be discussed in Chapter 2 of this document.

1.3 Research methodology

The research employs an experimental approach to evaluate the result of a simulated wind turbine and hydraulic transmission system. The simulation applied semi-empirical modelling of physical components that made up the hydraulic transmission and Savonius turbine systems. Matlab graphical interface (Simulink) is used for modelling and simulation.

The experiment made use of commercially available hardware components as shown assembled in Fig. 1. Virtual simulation model of turbine is used to control the input rotational speed of the

IEHEC motor. In practice, some of the input variables to the simulated model, such as pressure and flow rate are measured signals from the physical sensors in the experimental set-up. The results of the experiment will be compared to that of the virtual simulation model.

A plot of the turbine tip speed ratio and torque coefficient will outline the conformity and concurrence of the models while taking into account the assumptions and approximations used during modeling.

The virtual turbine model is compiled and run in real time interface of ControlDesk software (dSPACE – DS1005). The real time interface (RTI) feeds the operating parameters of the turbine to the inverter, and subsequently control the rotational speed of the IEHEC motor. Similarly, outputs from the set-up such as the pressure, temperature and volume flow of the pump are measured. The interconnectivity of the physical set-up and the ControlDesk is made possible by use of an analog to digital (ADC) and digital to analog (DAC) board for signal processing.

The experiment was carried out by initially operating the IEHEC motor at constant speeds while varying the valve orifice area over a fixed time period. By so doing, the temperature, pressure, flow rate and thermal power of the system were evaluated. Documentation and evaluation of the experimental results is outlined in the following Chapters. Of interests are pressure build up with changing wind speed in proportion to varied valve orifice area, thermal power of the system, flow characteristics of the valve and efficiency of the turbine. Figure 2 shows a schematic arrangement of the system set-up.

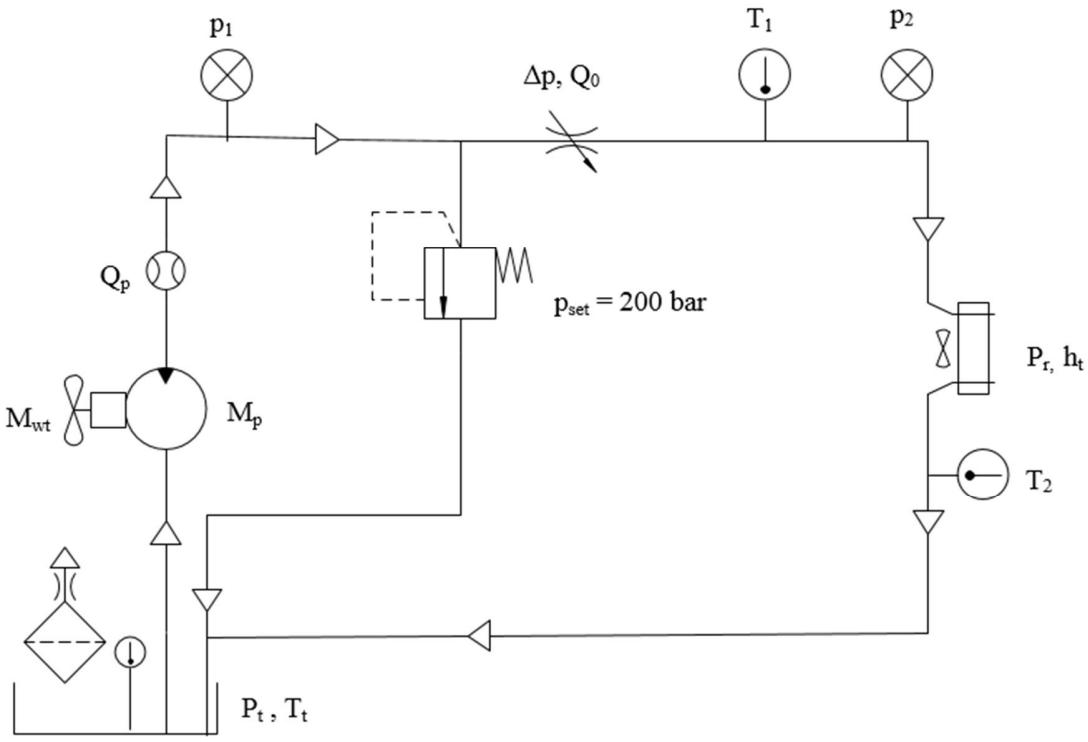

Figure 2. Schematics of assembly of system Hardware components.

1.4 Organization of the study

The outline of this thesis is as follows. In the second Chapter, the system components are introduced together with mathematical models used in system set-up. In Chapter 3, the turbine models will be reviewed. Modification to the virtual simulation model, experimental set-up and the measurement procedure will be explained. Following the measurement procedure are result tabulation and analysis in the fourth Chapter. Finally, the conclusion is drawn together with recommendations.

2 COMPONENT DISCRIPTION AND DIMENSIONING

This section discusses in brief the component description, dimensioning and parametric equations used in modelling the output responses of the input parameters to these components.

2.1 Savonius turbine model

The aerodynamic energy of wind is a function of the mass flow rate $\dot{m}$ and rate of change in the kinetic energy E of wind [12].

$$\dot{m} = \rho A v \tag{1}$$

$$E = 0.5 m_w v^2 \tag{2}$$

, where m_w is wind, v is the wind velocity, ρ density of the wind, A turbine cross-sectional area and E is the kinetic energy of wind.

From equations (1 & 2), wind power (P_w) [12] is derived.

$$P_w = \dot{m} \frac{dE}{dt} = \frac{1}{2} \rho A v^3 \tag{3}$$

, where $\frac{dE}{dt}$ is the rate of change in the kinetic energy of wind.

Equation (3) gives power contained in wind moving across the turbine's cross-sectional area.

Betz Criterion [13] presents an ideal wind energy conversion efficiency of a wind turbine. The limit stands at a maximum of 59 %. In practice, this efficiency level is hardly achieved as is visible in the Fig. 3. The power coefficient (C_p) [14, 15], which is dependent on the tip speed ratio of the rotor, is used to determine the efficiency of the turbine. A realistic C_p value lies between (0.35 – 0.40) % for practical wind turbines [13]. The power output of any wind turbine is a function of its power coefficient. Turbine power (P_{wt}) [12] is deduced.

$$P_{wt} = C_p P_w = M_{wt} \omega \tag{4}$$

, where M_{wt} is turbine output torque and ω is the angular velocity of the rotor. Hence turbine output torque M_{wt} is derived as follows:

Power coefficient (C_P) of a turbine is dependent on the turbine's tip speed ratio (λ) [16]. This relationship is given by

$$C_p = \frac{M_{wt}\omega}{\frac{1}{2}\rho A v^3} = C_t\lambda \quad (5)$$

, where λ is tip speed ratio and C_t is torque coefficient and M_{wt} is the turbine output torque. The system torque is defined by

$$M_{wt} = 0.5\rho C_t(\lambda)v^2 Ar \quad (6)$$

Tip speed ratio which is the ratio of the blade speed to free stream wind speed across the blade [16] is given by

$$\lambda = \frac{\omega r}{v} \quad (7)$$

, where *r* is the radius of the rotor blade.

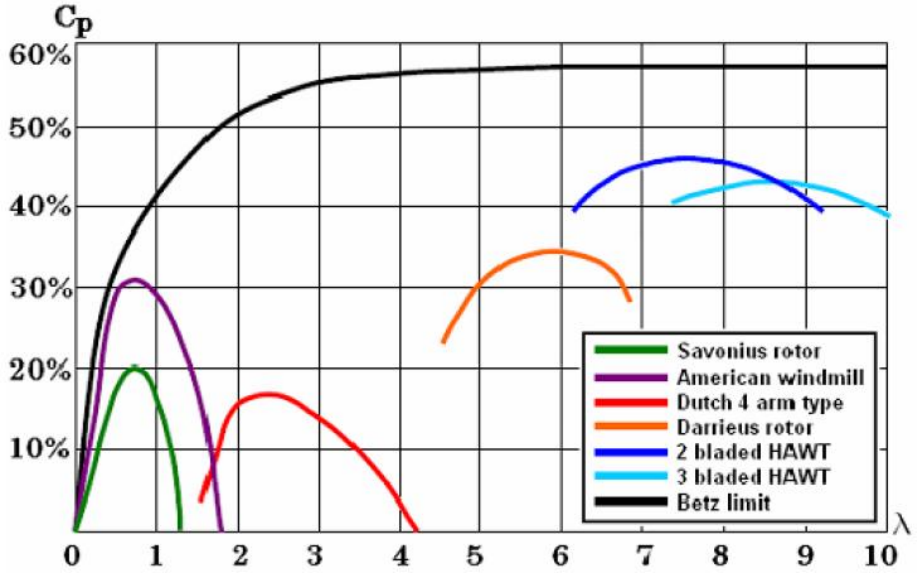

Figure 3. Power coefficient (C_p) versus Tip speed ratio (λ) of various Wind Turbines [17].

Of these turbines, Savonius rotor was chosen due to its high self-starting torque at low rotor speed [18]. This characteristic of the rotor makes for good application in low wind speed area. Due to low power efficiency of the Savonius rotor; with typical power coefficient in range of (12 – 15) % and tip speed ratio (λ) of 0.7% [19], different research has been carried out to this effect to improve performance.

Further experimental studies carried out on Savonius rotor has been documented showing efficiency improvement ranging from 20% to 35% [20, 21] corresponding to an optimal tip speed ratio of about 0.95. The variations in power coefficient arise from modification to geometrical parameters of conventional Savonius rotor [22]. By method of extrapolation and closed jet wind tunnel testing, optimum power coefficient of 32% has been achieved with modification in conventional Savonius rotor having central shaft. Similarly power coefficient of 21% has been documented in an open wind jet tunnel study of a Savonius rotor with a central shaft design modification [23]. Hence one can observe a significant impact on power output of the turbine with geometrical modification and test environment. By applying known torque coefficient parameter of conventional wind turbine, the power coefficients and consequently power outputs of the turbine could be evaluated.

Parameters of a prototype Savonius rotor was used to model a practical Savonius rotor for the experiment. Figure 4 shows torque coefficient and tip speed ratio relationship of Savonius turbine models.

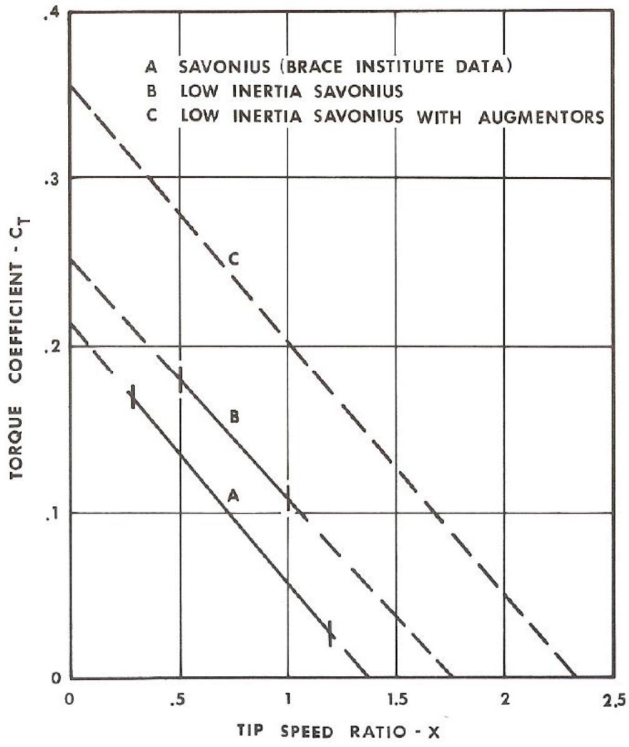

Figure 4. Torque Coefficient and Tip speed ratio relationship of Savonius rotor models [2].

The slope (line C) of low inertia Savonius rotor with augmentors was chosen. From this information, the equation of torque coefficient C_t of the rotor could be derived by applying equation of a straight line with negative gradient.

From the graph of Fig. 4, the straight line equation of slope C is deduced.

$$C_t(\lambda) = -KX(\lambda) + B(C_t) \quad (8)$$

, where B is the intercept along C_t axis, X is tip speed ratio parameter along (x) axis and K is the gradient of the graph.

2.2 IEHEC Motor

IEHEC motor is a permanent magnet synchronous electrical motor, consisting of integrated toothed-coil permanent magnet and axial piston hydraulic pump directly driven by the same shaft, this allows for operation in high pressure application. Performance evaluation carried out indicates an efficiency of about 95% at 150 Nm and 1000 rpm [24]. The control of the IEHEC is an electrical frequency converter for fast response in dynamic application and can be used both in pumping and motoring modes [25]. With its high efficiency and fast dynamic response, IEHEC motor's application is wide ranging and very suitable for integrated operations [24]. The fast dynamic response of this system stems from use of powerful electrical drive technology [26]. Displayed in Fig. 5 are sectional and side views of the IEHEC motor respectively. Table 1 outlines the system specifications.

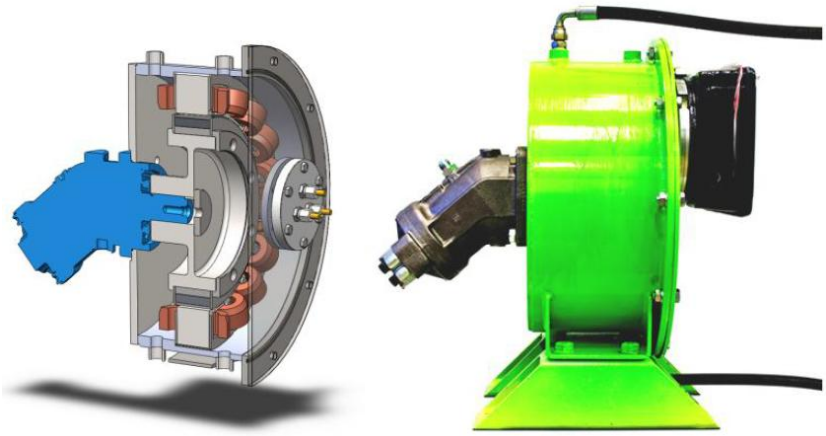

Figure 5. Sectional and side views of an IEHEC Motor [24].

Table 1. IEHEC motor Specification [24].

Parameter	**Value**
Length	398mm
Weight (EM + HM)	110kg (92kg + 18kg)
Nominal power	26 kW
Flow rate	Up to 180 l/min
Pressure	Up to 400 bar
Rated voltage	400 V
Nominal current	44 A
Coolant flow	4 l/min @ 70°C
Nominal speed	1500 RPM
Supply frequency at nominal speed	200Hz
Measured torque density at nominal point	4.4 Nm/Kg

In the study; the IEHEC motor mimicking the Savonius turbine is controlled with the parameters of the wind turbine. Speed signal from simulation interacts with the frequency converter which in turn defines the speed of the motor. Using Newton's second law for rotation, angular acceleration of wind turbine is defined [27].

$$\ddot{\theta} = \frac{M_{wt}+M_p}{J} \tag{10}$$

, where *J* is the rotor Inertia. By integrating the angular acceleration, the angular velocity is achieved.

$$\int \ddot{\theta} = \omega \tag{11}$$

Inertia of the rotor is defined by:

$$J = 0.5mr^2 \tag{12}$$

, where *m* is the mass of rotor.

The pump input torque (M_p) [28] is given by

$$M_p = \frac{V_k \Delta p_p}{2\pi} \quad (9)$$

, where p_p is the pump pressure and, V_k is the fixed volume displacement of the integrated pump of the IEHEC motor rated at 63 cm3/rev.

It should be noted that the pump input torque M_p is a resistance torque, hence opposes the rotational speed of the turbine. Figure 6 presents a typical Savonius rotor design where *D* and D_o are the internal and external diameters of the blades respectively, *d* is the radius and *c* represents the distance between the ends of the blades at the point of connection to the central shaft. For more information about turbine dimension parameter used in the design, see Appendix 1. It should be noted that the mass used in simulation models is 362 kg.

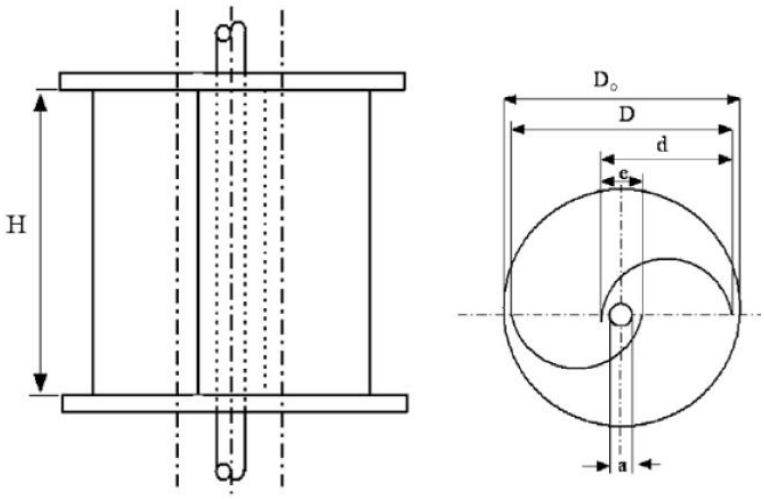

Figure 6. Illustration of a single-stage Savonius rotor [29].

2.3 Valves

Valve is one of the principal components used in hydraulic systems. Applications range from flow control to pressure control applications. In the system set-up, both valve types were used. These include a throttle valve and a pressure relief valve. For simplicity, the focus of this

Chapter will be on the throttle valve. A brief introduction of the pressure relief valve will be highlighted.

2.3.1 Pressure relief valve

As a matter of safety, pressure relief valves are required in any hydraulic system where the source pressure could exceed the pressure calibration of components downstream of the hydraulic circuit. Otherwise in a situation where a specified pressure level should not be exceeded. Where fixed displacement hydraulic pump is used as is the case in this set-up, it is recommended the use of pressure relief valve alongside [30]. In these cases, the pressure relief valve set-point is set to open and bypass the excess pressure to the tank to avoid overload. The set-point at which the valve spring force equals the pressure force and valve starts to open is referred to as the cracking pressure [31]. Hence:

$$p_c = \frac{F_{S0} \pm F_c}{A_v} \tag{13}$$

, where p_c is the cracking pressure, F_{s0} is spring force preload = (k_s*x_0), F_c is coulomb friction force and A_v is poppet area normal to pressure.

A typical direct acting pressure relief valve is presented in the Fig. 7.

To maintain a constant flow rate in the system, the calibrated valve pressure set point of 200 bars must not be exceeded. Hence operation within this pressure limit ensures that the system is safe.

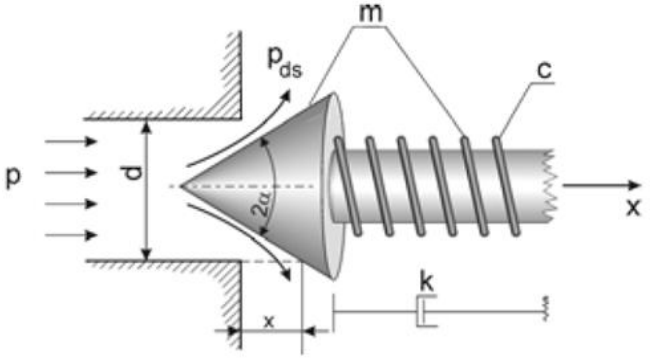

Figure 7. A direct acting pressure relief valve, where p_{ds} is discharge port pressure, k is viscous force coefficient, x is poppet displacement, m is mass of the moving parts, d is diameter of orifice and c is spring stiffness [32].

2.3.2 Hydraulic throttle orifice

One of the vital components of the system set-up, responsible for flow regulation, and subsequently, torque vis-à-vis, pressure build-up and thermal power generation is the flow control pin valve. This valve uses a throttle mechanism through which fluid flow is constricted by adjusting the valve stem. This results in pressure differential across the valve. Application of high velocity short throat orifice when working with high pressure fluids aimed at achieving high pressure drop is common practice. This serves to limit the risk of cavitation, erosion to the valve components and damaging shock wave in the system when working with fluid susceptible to flash [33].

Though the focus of this study is not to seek to improve the design performance of the throttle valve, it is worth outlining that high velocity flow of fluid through the orifice is the bane of controlling valve operation. Hence the operating characteristics, operating limit and operation life of the valve should be considered.

The pin valve used in the set-up is a DV Series flow control valve. DV-16 is an inline mounting valve of schematics in Fig. 8. See Appendix 2 for more manufacturer's information on valve dimensioning.

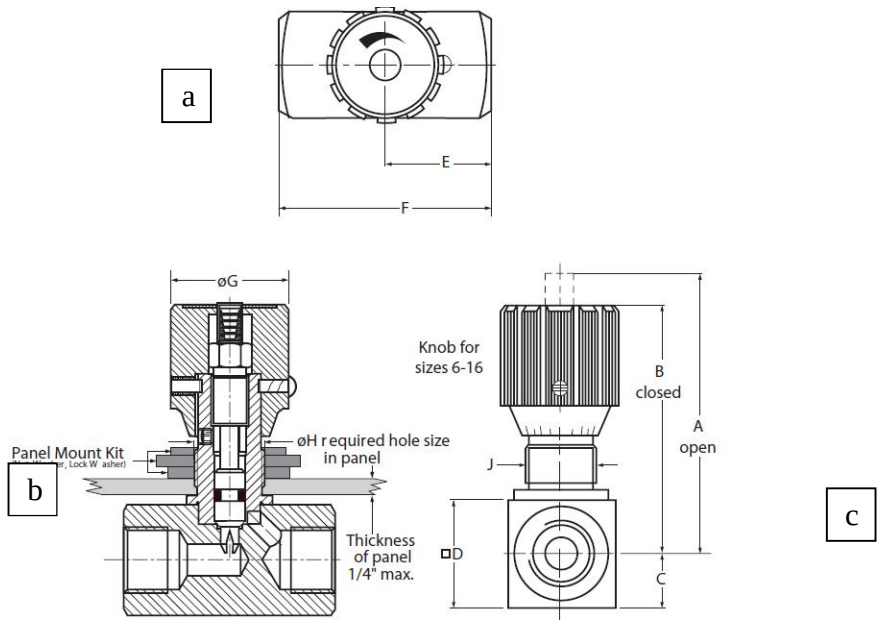

Figure 8. DV-16 needle valve diagram (a) Top view (b) Sectional view (c) front view [34].

2.3.3 Throttle Valve Mechanism

The valve in question is a manually operated pin valve. By turning the control knob of the valve, hydraulic flow could be regulated. Starting from closed position, the valve is opened by turning the valve knob anti-clockwise and closed by turning in clockwise direction. Calibration on the on the knob allows for repeatability of the process.

Among parameters of the valve to be measured are the semi-empirical flow coefficient (K_v) detailing flow characteristics with each number of turns of the valve knob and the orifice diameter of the valve. Using orifice volume flow equation [35], the orifice area (A_o) could be calculated, thus:

$$A_o = \frac{Q}{C_d\sqrt{(\frac{2}{\rho_{oil}}\Delta p)}} \tag{14}$$

, where Q is volume flow across valve (measured using flow sensor), Δp is pressure difference across valve, C_d is non-dimensional parameter; the orifice discharge coefficient approximately 0.61 for circular valve orifice geometry, and ρ_{oil} is the oil density [kg/m^3].

Similarly, the semi-empirical flow coefficient of the valve (K_v) depicting flow and pressure drop relationship could be evaluated [36].

$$K_v = Q\sqrt{(\frac{\rho_{oil}}{\Delta p})} \tag{15}$$

Thermal power (P_k) is generated as fluid passes through the constricted valve. The power generated is a function of fluid flow rate and pressure drop across the valve [35].

$$P_k = Q\Delta p \tag{16}$$

Figure 9 demonstrates the behavior of flow through the throttle orifice, where p_1 is inlet pressure, p_2 is outlet pressure, v_1 is inlet fluid velocity, v_2 is fluid velocity across the orifice and d is orifice diameter. At low velocity, flow is laminar and turbulent with increasing velocity.

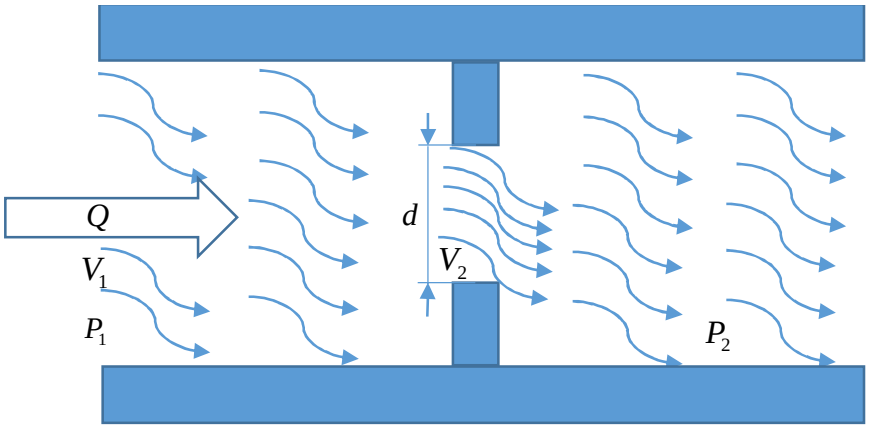

Figure 9. Cross-section of flow through a throttle orifice.

2.4 Sensors

This section is dedicated to the sensors used in the system set-up. These include the flow meter, pressure and temperature sensors. With these sensors, the flow rate, temperature and pressure can be measured.

2.4.1 Flow meter

Flow meters are used basically to measure the amount of fluid flow per time period. In the set-up, a gear type flow meter is used. The fluid flow that passes through, drives a non-contact gear which is measured by an in-built sensor as the gear rotates by one tooth pitch. The signal produced is pre-amplified. The sensor uses a two-channel sampling for better resolution and indication of flow direction. Figure 10 shows flow meter component with its constituent parts. See Appendix 3 for more information of Flow Meter VC flow characteristics

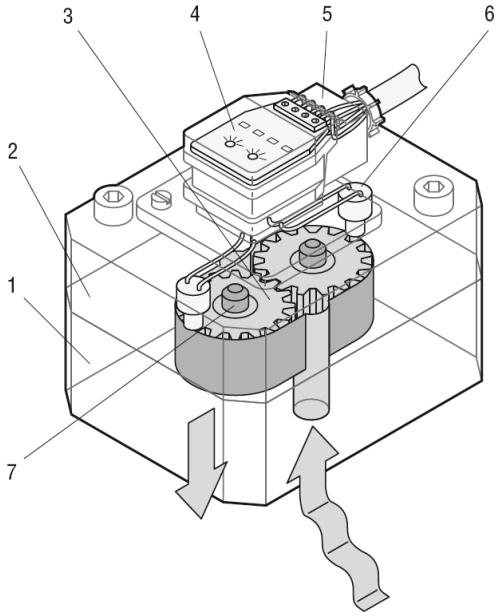

Figure 10. KRACHT flowmeter: 1) Housing 2) Cover 3) Gear 4) Preamplifier 5) Connector 6) Sensor 7) Bearing assembly [37].

Table 2. The general characteristics of the KRACHT flowmeter [37].

General Characteristics	
Design	Gear motor
Connection type	Plate mounting / pipe connection
Mounting position	Optional
Flow direction	Optional
Viscosity	1... 1.000.000cSt, /according to series)
Max. pressure drop	Δp_{max} = 16 bar / 230 psi

2.4.2 Pressure Transducer

Pressure is the measure of force acting on a given surface area. To measure the pressure in the hydraulic fluid, pressure sensors were used in the experimental set-up. These were positioned as such to measure the inline (before the valve) and return (after the valve) pressure. From these measured outputs, the pressure difference across the valve could be calculated. The data from

the pressure sensor in the inline side is same as the pressure difference of the pump. This data is fed into the pump model to simulate the response of pump torque with increasing pressure.

Figure 11. HDA 3845 pressure transducer [38].

Used in the set-up is a Hydac HDA 3845 pressure transducer. The accuracy of this component is dependent on the temperature of the fluid. See Appendix 4 for manufacturer's technical and dimension information of component.

2.4.3 Temperature Sensor

This component is used to measure the temperature of the fluid in the system. The sensors were positioned to measure the temperature of the fluid as it emerges from the valve in the return pressure line and another after the fluid has been cooled. This information provides knowledge of how much heat is dissipated and the temperature of the fluid returning to the oil tank. Used in the set-up is a Hydac 320 series temperature transducer. See Appendix 5 for manufacturer's technical information of component.

Figure 12. HYDAC 320 series electronic temperature switch [38].

2.5 Cooler

Heat exchangers (coolers) perform the function of temperature exchange between two fluids without them coming into contact. The use to which they are put, either to collect or dissipate heat from a body depends on the need of application. There exist various kinds of heat exchangers in commercial application. In this experiment as has been outlined earlier, the heat exchanger is to dissipate the heat generated in the hydraulic fluid and used for house heating.

An oil to air heat exchanger operating on the mechanism of force convective heat transfer was used. The off/on controlled fan of heat exchanger is equipped with a 0.25 kW rated motor operating at 50 Hz (3000 RPM) maximum fan rotor speed. By Newton´s law of cooling, the radiative power P_r of the cooler can be derived [39].

$$P_r = h_t A_r (T_f - T_a) \tag{17}$$

, where h_t is convective heat-transfer coefficient of the radiator [W/m^2 ^{0}C], A_r is radiative area [m^2], T_f is final oil temperature [^{0}C] corresponding to the radiator plate temperature and T_a is the ambient air temperature [^{0}C].

Figure 13. Forced convective oil to air cooler.

However, theoretical approach is deemed more suitable to analyze the result of the cooling unit. Calculations is carried out using parameters of a known oil cooler to estimate the heat output of the system. This is due to unavailability of manufacturer's performance characteristic information of the cooler used in the set-up (see Fig. 13) and thus, accurate results cannot be guaranteed. In addition, short experiment time and low oil temperature difference recorded in the pre-trial experiment makes the use of the cooler barely relevant. The amount of heat generated in the fluid is attributed to the volume of oil used and short time span of the experiment cycle.

The heat load (P_h) of the system over an operating time period is expected to tally that of the turbine power as no work is done by the hydraulic fluid in the system [11]. This is derived thus:

$$P_h = \frac{V(T_f - T_\infty)}{60\Delta t} \tag{18}$$

, where: V is the tank volume [m^3], Δt time period over temperature measurent [s], and T_∞ is ambient oil temperature [°C]. Using this approach, it is assumed that the final oil temperature (T_f) corresponds to the radiator plate temperature at the elapse of experiment time.

To choose a suitable radiator, the power loss P_v is evaluated using the equation as given [40].

$$P_v = \frac{V\rho_{oil}C_{voil}(T_f - T_\infty)}{60\Delta t} \quad (19)$$

, where ρ_{oil} is density of the oil; for mineral oil: 915 kg/m^3, C_{voil} is specific heat capacity of oil; for mineral oil 1.88 kJ/kg°C. For a given air temperature T_1 [°C] and a desired oil temperature of T_2 [°C], the specific cooling capacity P_{sc} [kW/°C] of the cooler could be calculated by [40]

$$P_{sc} = \frac{P_v}{(T_2 - T_1)} \quad (20)$$

2.6 Hydraulic Oil

Hydraulic fluid is a vital element of any hydraulic operating system. Hydraulic fluids have found application in forestry, marine and more frequent in mobile equipment for power transmission, wear protection, cooling and heat transfer.

One of the underlying hydraulic fluids' properties that determine its suitability is its viscosity-temperature behavior. The relationship is inversely proportional with increasing or decreasing fluid temperature [41]. High viscosity index ensures wide temperature operating range of the fluid. Other properties required of good hydraulic fluids are low compressibility, low foaming tendency, high oxidation stability over a time period, tribological compatibility with materials, environmental impact and many others [42, 43].

Leakages and pressure loss in hydraulic components are common problems of pressurized systems. With hydraulic oil, these problems are exacerbated by cavitation and oil viscosity [44]. With about 9% air content in solution of mineral based hydraulic oil under atmospheric condition, cavitation in the fluid affects the dynamic power transmissibility of the fluid [44] and hampers the performance of the components in the system.

In use in the experiment is mineral based hydraulic oil HVLP 46 was used for its durability, availability in various viscosity grades, toxicogical behavior, hydrolytic stability and good thermal property in power transmission and heat transfer application. It is recommended to operate at permitted viscosity drop of 15 %, at temperature reaching 100°C [41]. Presented in Fig. 14 and Fig. 15 are the properties and viscosity – temperature relation of HVLP 46 hydraulic

oil. A high viscosity index indicates a small change in viscosity with changes in temperature and low index means a large viscosity change with change in the oil temperature.

As is the case with any moving substance in contact with itself and other substance, friction is ever present. In flowing hydraulic fluid, friction contribute to the temperature rise in the system. More so, compression and expansion of the fluid as it passes through the valve increases the intermolecular activity present which results in stresses and tearing of molecular chains to add more heat to the fluid [11].

Ultramax HVLP 46	
Colour	yellow
Viscosity, mm^2/s @ 100 °C. ASTM D-445	8,1
Viscosity, mm^2/s @ 40 °C. ASTM D-445	46
Viscosity Index ASTM D-2270	148
TAN; mg KOH/g ASTM D-664	0,6
Pour Point, °C ASTM D-5950	-45
Specific Gravity @ 15.6°C. ASTM D-4052	0,858
Flash Point, COC, °C. ASTM D-92	225

Figure 14. Hydraulic oil HVLP 46 properties [43].

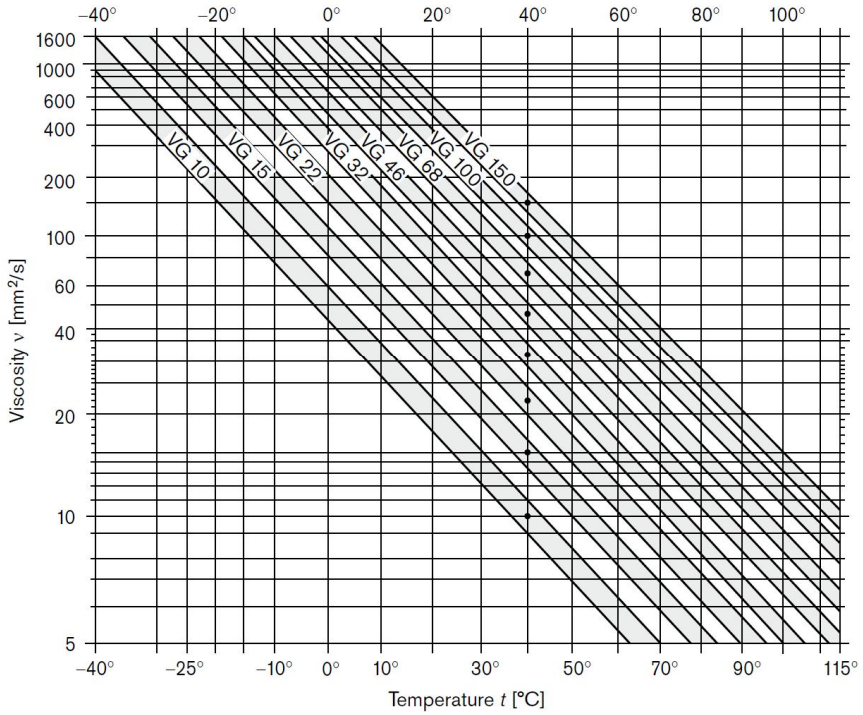

Figure 15. Viscosity – temperature diagram (VI 100, double logarithmic representation) [41].

2.7 Oil reservoir

The oil reservoir in use is a steel enclosed tank measuring up to 300 liters in capacity. The primary function of the tank is storage and recirculation of the hydraulic fluid. Connected to the tank are the suction line to the pump and the return line as represented in Fig. 16.

Figure 16. Hydraulic oil tank.

Other than hydraulic fluid storage, the tank also serves as a heat storing component. The undissipated heat in the return oil infinitesimally accumulates thereby raising the temperature of the fluid in the tank. Owing to the material of the storage, energy is loss through conduction. This energy could be made useful if tapped and used for floor eating. This implies close proximity of the storage tank to the target usage area.

The phenomenon of heat accumulation in the tank is described by tank oil temperature T_t as given [1].

$$T_t = \frac{P_t}{\rho_{oil} * V * C_{voil}} + T_\infty \tag{21}$$

Similarly, the tank thermal energy P_t (in the oil returning to the tank) could be calculated.

$$P_t = P_k - P_r \tag{22}$$

3 EXPERIMENTAL DESIGN

In this Chapter the experimental simulation, system set-up and system control is described. The virtually simulated model of system from previous study in relation to the laboratory experimental process is briefly explained. The interaction between the hardware components, signal processing and integration of hardware of real time interface (dSPACE) with Matlab/Simulink software in the experiment is outlined.

3.1 Virtual simulation model

Encompassed in the virtual simulation model are equations representing the different components that make up the circuit. The rotor is the power source for driving the hydraulic pump. Other parts modelled include the throttle valve, pressure relief valve, oil to air heat exchanger and hydraulic fluid storage tank. The fluid power circuit was modelled and simulated in Simulink using semi-empirical modelling method.

In the earlier study of the system, two different torque coefficients (C_t) were applied in the virtually simulated system model to test for optimum orifice diameter at which power output is maximized. It was determined from calculation and test simulations that the optimum orifice diameter of the model is a function of the turbine's tip speed ratio which depends on the wind speed and load on the turbine (pump torque). This relationship is given in Fig. 17. From the outcome of this test, the turbine was found to operate optimally at torque coefficient of 0.35. [1] This claim is the focus for verification of the modelled turbine's optimum torque coefficient parameter. To harness optimum power from the wind, the throttle orifice has to be adjusted to achieve an optimum tip speed ratio of the turbine.

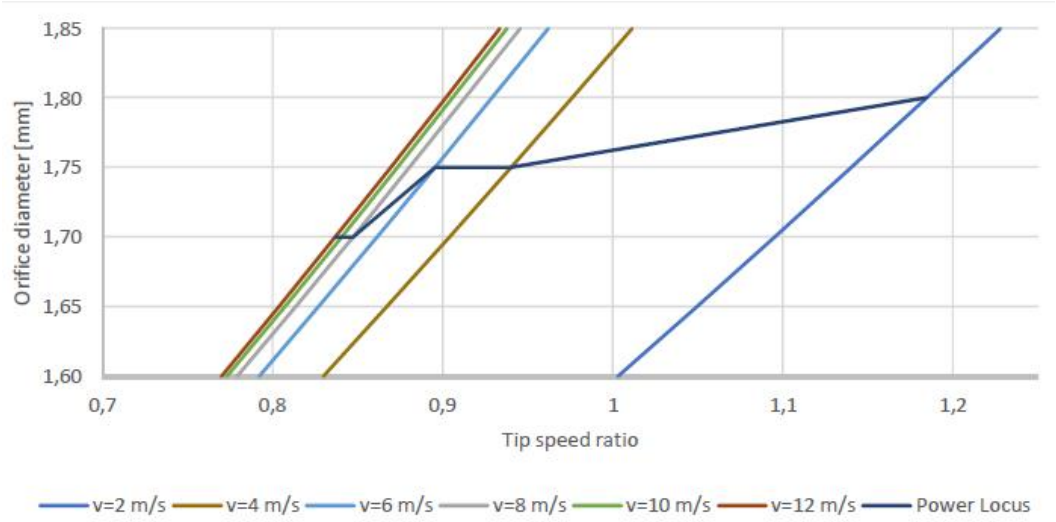

Figure 17. Tip speed ratio relationship with orifice diameter [1].

3.2 Hardware-in-the-loop simulation

The experiment is designed by method of HIL simulation. The virtual turbine simulation model is used in tandem with the experimental system hardware set-up. A sample wind profile of constant wind speeds (2 m/s to 12 m/s) over a 30 minutes time period was designed to run in the simulation. System pressure input parameter was measured directly from the system responses using sensor. The pressure variable determines the pump output torque. Imbedded equations calculates turbine's tip speed ratio and torque coefficient. These parameters controls the motor's speed.

3.3 Experimentation

The experiment made use of commercially available hardware for system set-up. The rotational speed output signal of the virtual Savonius turbine model controls the speed of the IEHEC motor which drives the pump. Simulation was set to infinite time and stopped at the elapse of wind speed data sample time.

Connected to the integrated motor unit is a frequency converter which varies the frequency of the motor with change in the rotational speed of the turbine model. This variation is as a result of change in the wind speed. The dSPACE hardware interacts and processes input sensor signals in the system set-up in real time.

The experiment is carried out by controlling the motor with the designed turbine model while regulating the valve orifice. The valve is increasingly opened by turning the valve knob anti-clockwise till full opening. The valve knob is calibrated between 0 to 9 numbers of repeatable turns. The valve knob for the experiment were set to 2, 3, 4, 5, 6 and 7 number of turns and their corresponding orifice diameters were measured and documented in the result chapters.

Having established the relationship between optimum throttle orifice with respect torque coefficient and wind speed, the Savonius turbine model of slope C in Fig. 4 and Eq. 8 depicting the torque coefficient of the turbine were applied in the turbine torque model.

Preliminary tests were carrid out to verify the pressure limit of the system. This is to ascertain that the system does not exceed the 200 bar pressure limt. To this effect, the system could be said to maintain a constant volume flow at any given time throughtout the system. Displayed in Fig. 18 is an assemly of the harware components of the system.

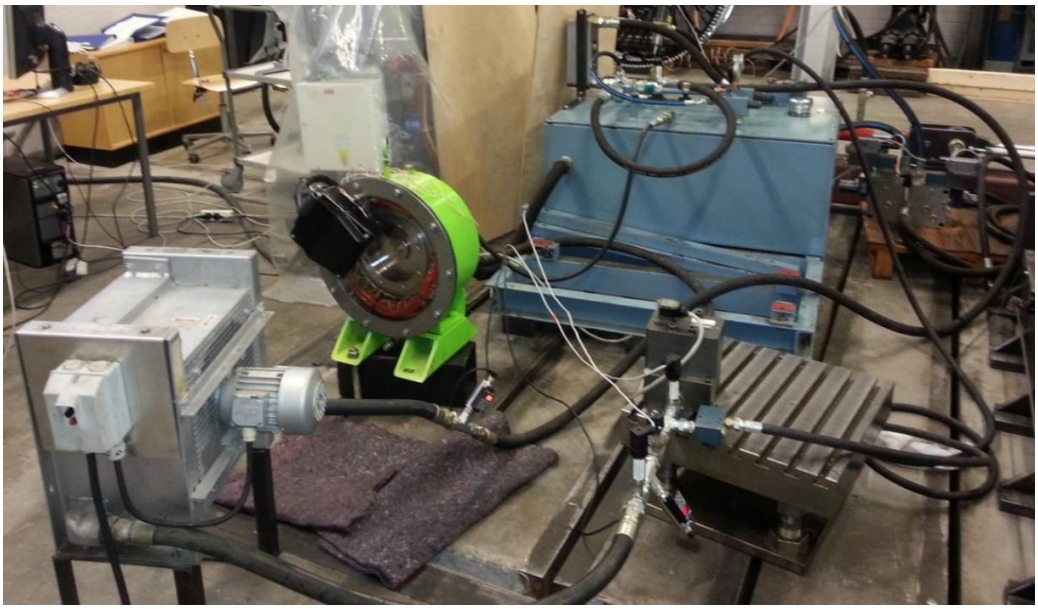

Figure 18. Experimental system hardware set-up.

4 RESULTS AND DISCUSSION

This Chapter presents the results of the laboratory experiments. The virtual simulation and test bench results from previous study [1] are presented as well. Analysis and comparison of results is carried out to verify prior inferences. Similarly, the throttle valve characteristic behavior of the valve manufacturer is compared with the simulated characteristics. Emphasis is laid on the valve optimum orifice diameter in relation to tip speed ratio, torque coefficient and thermal power output.

4.1 Virtual simulation result

The objective of presenting the result of the virtual simulation is to investigate correlation with the experimental results. As mentioned earlier, variations exist in the parameters used in these two models. One variation is the wind speed data used in the virtual simulation as recorded by the Finnish meteorological institute (See Fig. 19)

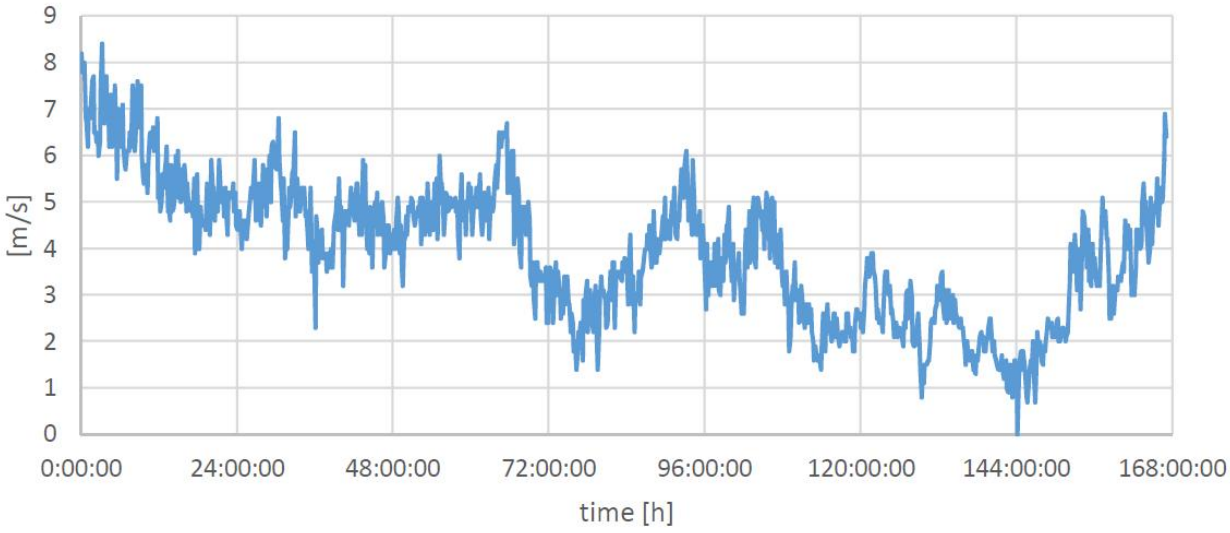

Figure 19. Wind speed data applied in virtual system simulation [1].

The optimum orifice diameter used in the models varied as well. These parameters (wind data and orifice diameter) used in the experiment is sampled in the virtual simulation as well. Average of the wind speed data was used to calculate the optimal orifice diameter used in the

test bench and as well to compute the output results of the virtual system recorded in Table 3 [1].

Two torque coefficients were simulated in the virtual simulation. The result of the simulation claims optimum torque coefficient C_t = 0.35, having higher power output. This torque coefficient parameter is subjected to scrutiny in the experimental Savonius turbine model.

Table 3. Calculated power values from the wind data [1].

Torque coefficient (C_t)	0.25	0.35
Average wind speed [m/s]	3.95	
RMS of wind speed [m/s]	4.44	
Power of average wind speed [W]	14.7	28.3
Power of RMS wind speed [W]	21.0	40.5
Simulated power of rotor [W]	22.8	41.6
Total power produced by average wind speed [W]	2453.3	4731.4
Total power produced by RMS of wind speed [W]	3505.8	6761.3
Total simulated power [W]	3803.8	6946.7
Total power production per annum (RMS) [kW/a]	183.9	354.7
Total simulated power production per annum [kW/a]	19.5	364.4

4.1.1 Virtual system optimum parameters evaluation

The supposed optimal orifice diameter of 1.85 mm was applied in the virtual rotor simulation at optimum torque coefficient C_t = 0.35 under constant wind speed v =10 m/s to verify the output value presented in Fig. 20.

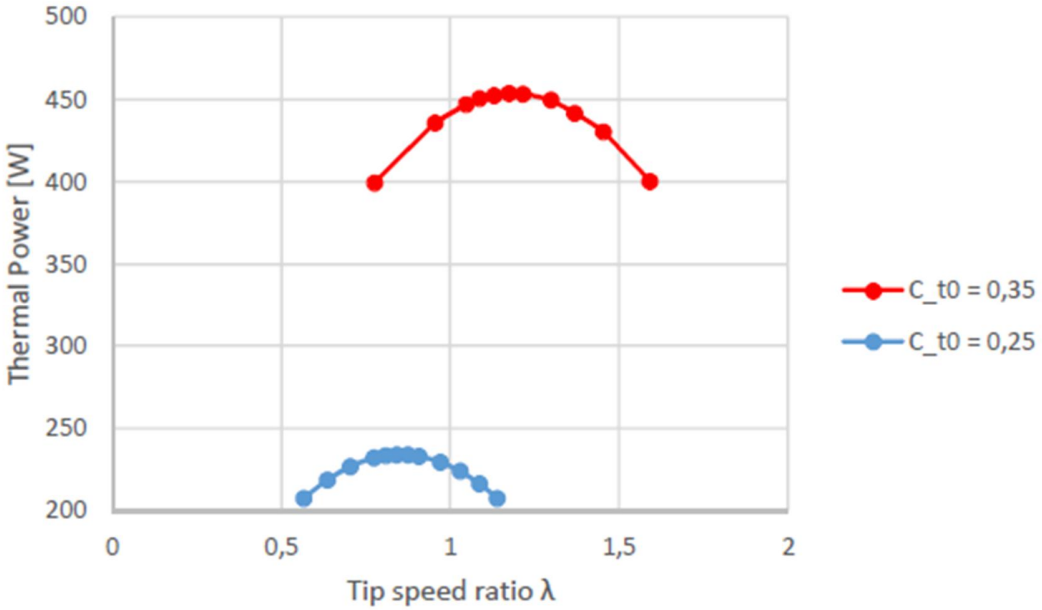

Figure 20. Tip speed ratio – power relationship of Virtual turbine model [1].

An assessment of the presented result (Fig. 20) was carried out using constant wind speed over time. The parameters of the virtually simulated system (optimum orifice diameter of the virtually simulated throttle orifice simulation at wind speed of 10 m/s and torque coefficient of 0.35) inputted gave rise to the result displayed in Fig. 21. From this result, the claimed optimum tip speed ratio of 1.17 in previous study [1] was not achieved. Similarly the torque coefficient of 0.35 was not achieved. Figure 22 shows that at cut-in wind speed of the turbine, the torque coefficient started to decline from initial value of 0.35. Output power of the turbine is not optimal at this point.

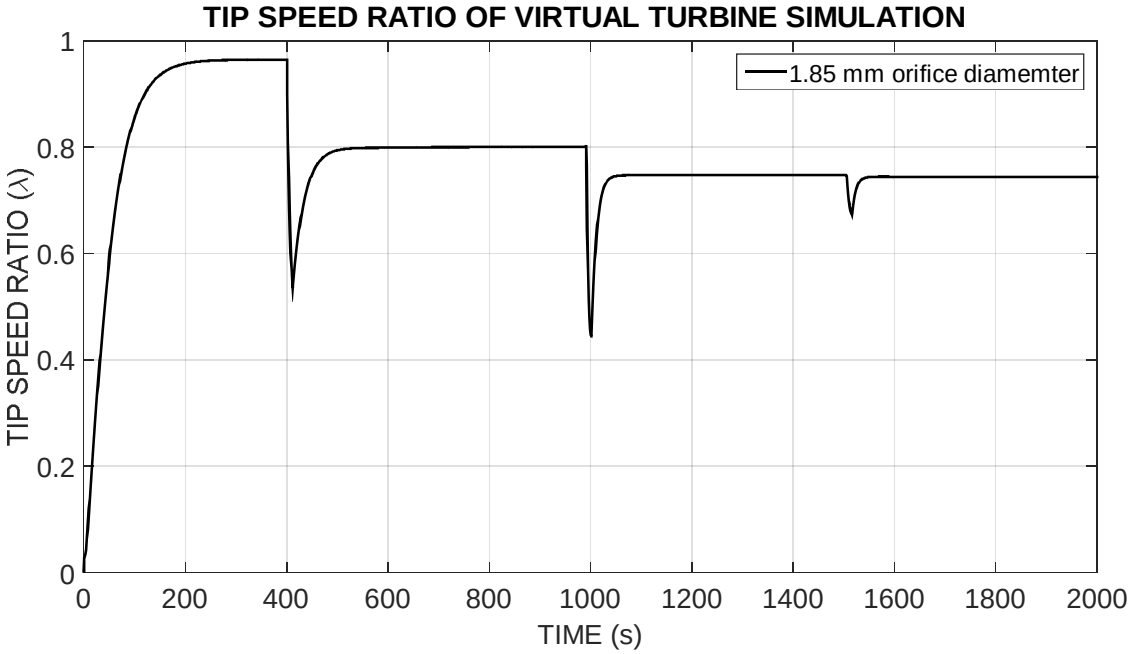

Figure 21. Tip speed ratio of Virtual turbine model.

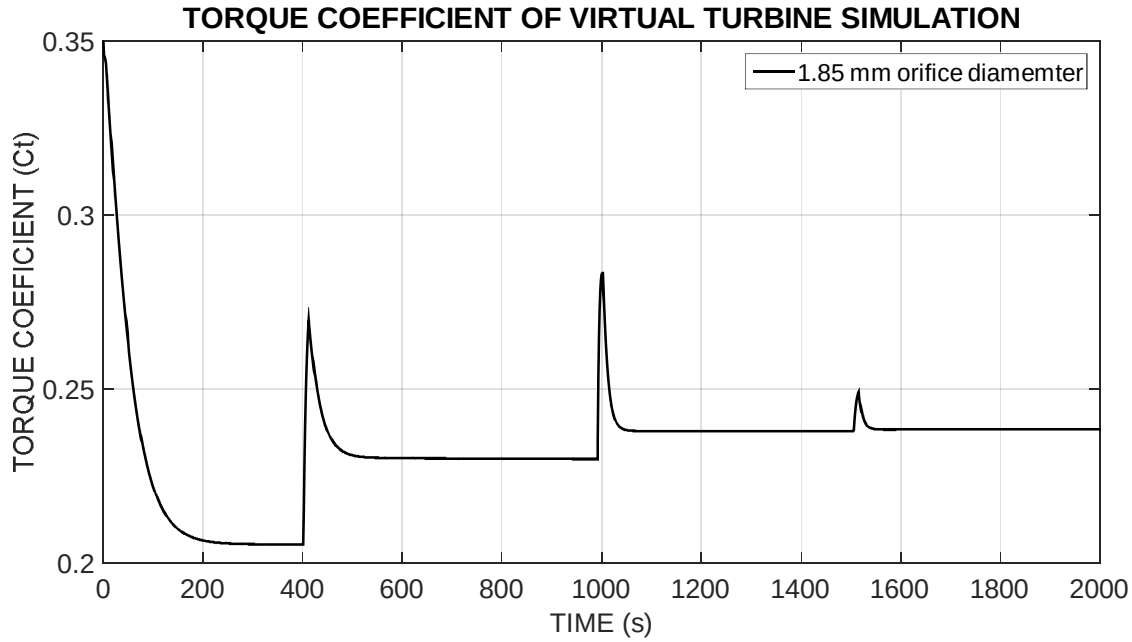

Figure 22. Torque coefficient of Virtual turbine model.

4.2 Test bench simulated result

Test bench from previous research is similar to the experimental set-up with some modifications. It served the purpose of empirical research to examine the parametric effect of generated power and optimal tip speed ratio of the system using two different torque coefficient values of the turbine [1]. A constant wind speed of 10 m/s was used in simulation. The optimum orifice diameters at the different torque coefficients were noted as well. Owing to the similarity in the two models (Test bench and laboratory experimental models), the results at the same operating conditions are more readily compared.

4.2.1 Turbine power and tip speed ratio characteristics of test bench model

By adjusting the throttle orifice in the test bench set-up, it was reported that optimal throttle orifice of 2.5 mm was reached for turbine simulation with torque coefficient of 0.35. Similarly, the optimal tip speed ratio which is wind speed dependent is achieved [1].

The Result of the study as presented in Fig. 23 shows an optimal tip speed ratio of 1.17 was reached for rotor of torque coefficient C_t = 0.35 and 0.84 for rotor of torque coefficient C_t = 0.25. However going by graph C of Fig. 4 depicting torque coefficient and tip speed ratio relationship of the Savonius turbine model used, the corresponding torque coefficient at tip-speed ratio of 1.17 is below 0.2. To investigate further, parameters of the test bench is configured in the virtual system simulation and result evaluated.

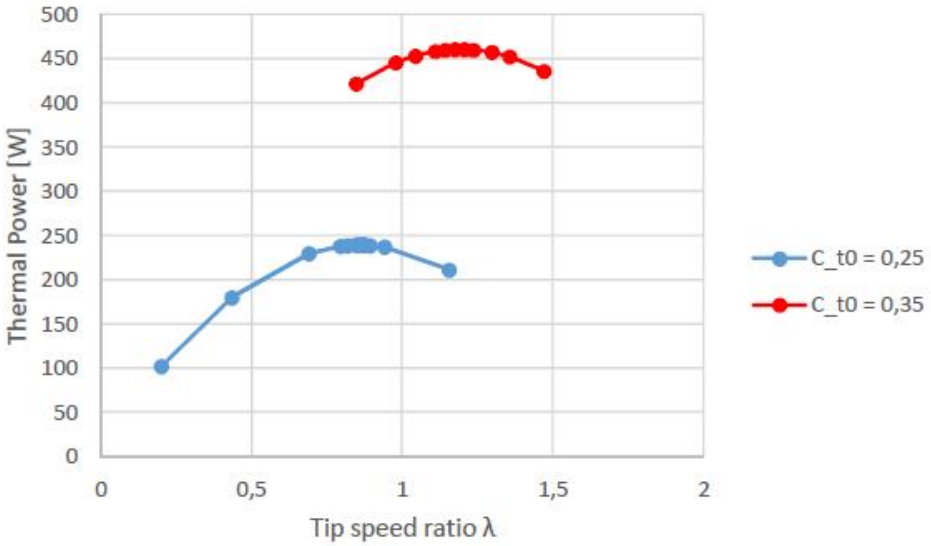

Figure 23. Effect of optimal tip speed ratio for different torque coefficient on power output [1].

4.2.2 Test bench optimum parameters evaluation

Using constant wind speed profile shown in Fig. 24 and test bench parameters (optimum valve orifice diameter of 2.5 mm and torque coefficient C_t = 0.35), the tip speed ratio and corresponding torque coefficient were presented in Fig. 24 and Fig. 25 respectively. Emphasis is laid on the response of the system in wind speed range of 10 – 12 m/s. Tip speed ratio of 1.19 was recorded. This is close to the claimed optimum value of 1.17. Similarly, the corresponding torque coefficient is below 0.2. With these two results, it can clearly be said that the torque coefficient applied in the virtual design is not optimum at 0.35. It is evident that torque increases with increasing wind speed. The fast change in turbine torque coefficient is as a result of pump load on the turbine. Hence the turbine output torque and pump input torque equalizes with time. This result is compared with the experimental simulation.

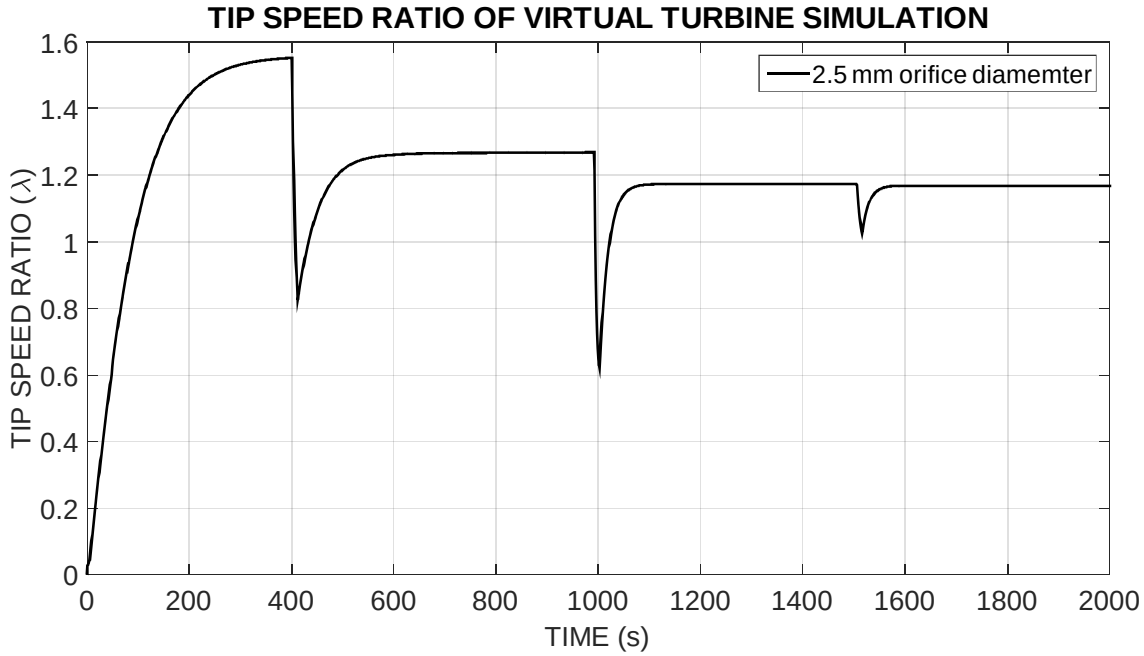

Figure 24. Tip speed ratio evaluation using test bench parameters.

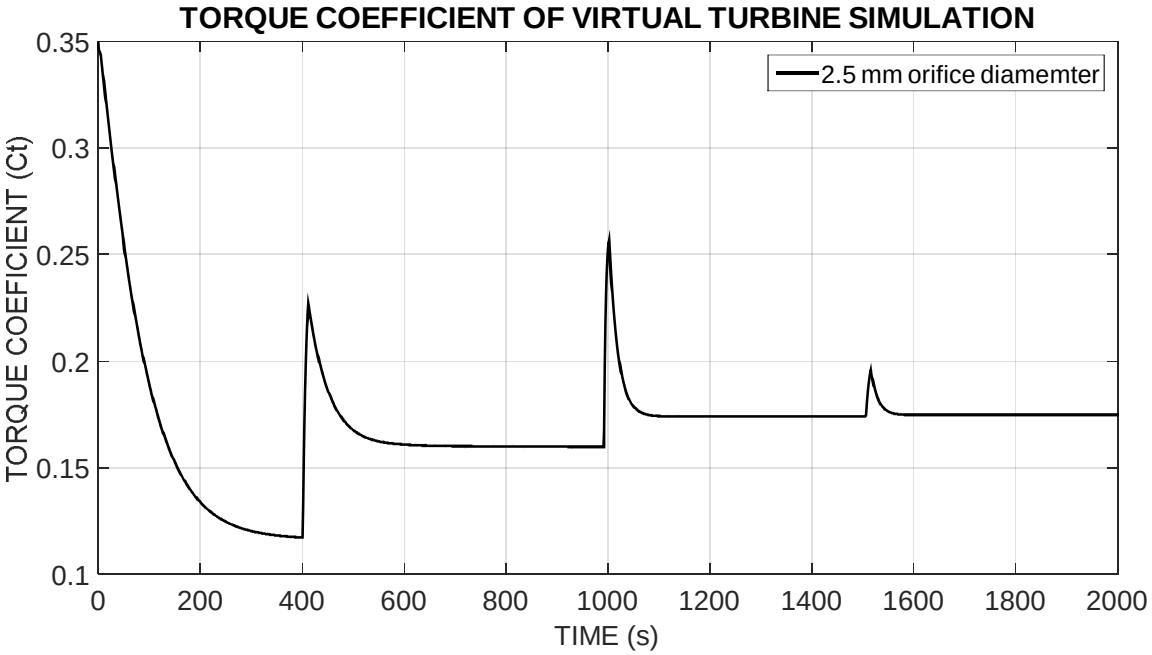

Figure 25. Torque coefficient evaluation using test bench parameters.

4.3 Experimental results

The results of the experiment is tabulated in the following Chapters. The Wind speed data used and subsequently turbine speed is presented in Fig. 26 and Fig. 27 respectively. The deviation noticed in the wind speed at 2 valve turns is as a result of time off-set during data recording. Same wind speed profile was used throughout the experiment. Only the extreme valve setting (2 and 7 turns) results were repesented due to the similarity of results at different orifice setting. This off-set is also noticed in some other results such as the torque coefficient, wind and system power outputs.

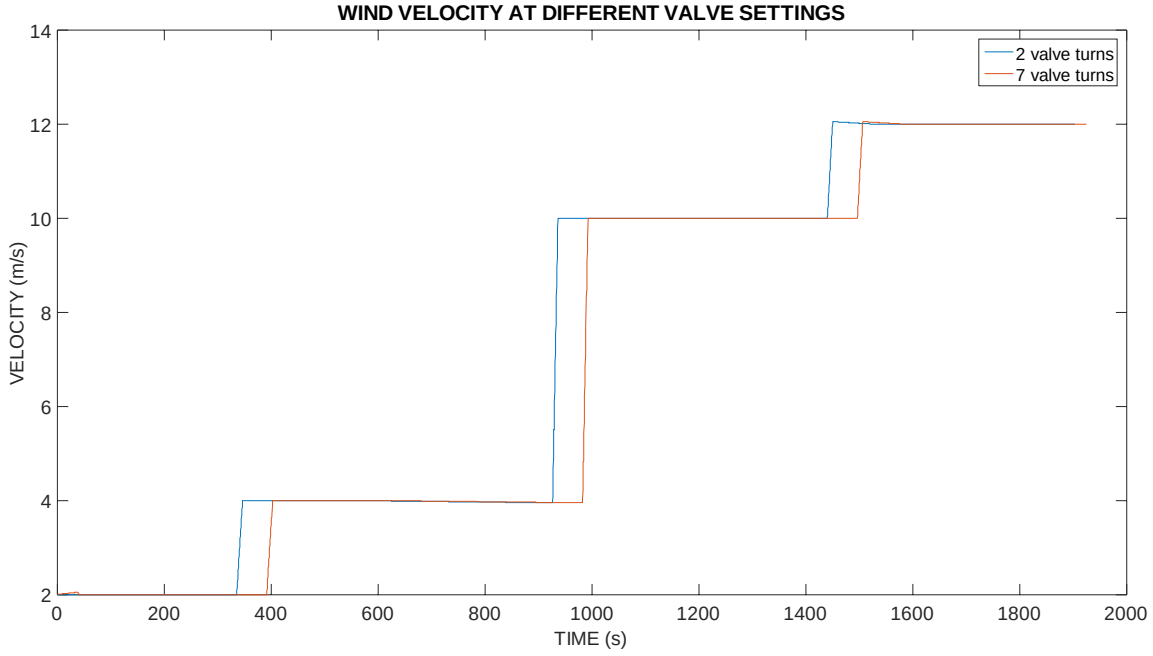

Figure 26. Wind speed profile.

The turbine was monitored to ensure that its operating speed is within the rated limit of the IEHEC motor of 1500 RPM. Upper speed limit of the experimental turbine was set to 1400 RPM. Other measures taken to ensure safety includes an emergency switch to halt operation. Unlike conventional Savonius turbine which rotates in either direction of the wind force, the experimental turbine model is subject to one directional rotation due to open-loop hydraulic circuit. The rotation of IEHEC motor was permitted only to other direction Maximum recorded speed of the turbine at 7 opening turns of the valve knob stands approximately 500 RPM.

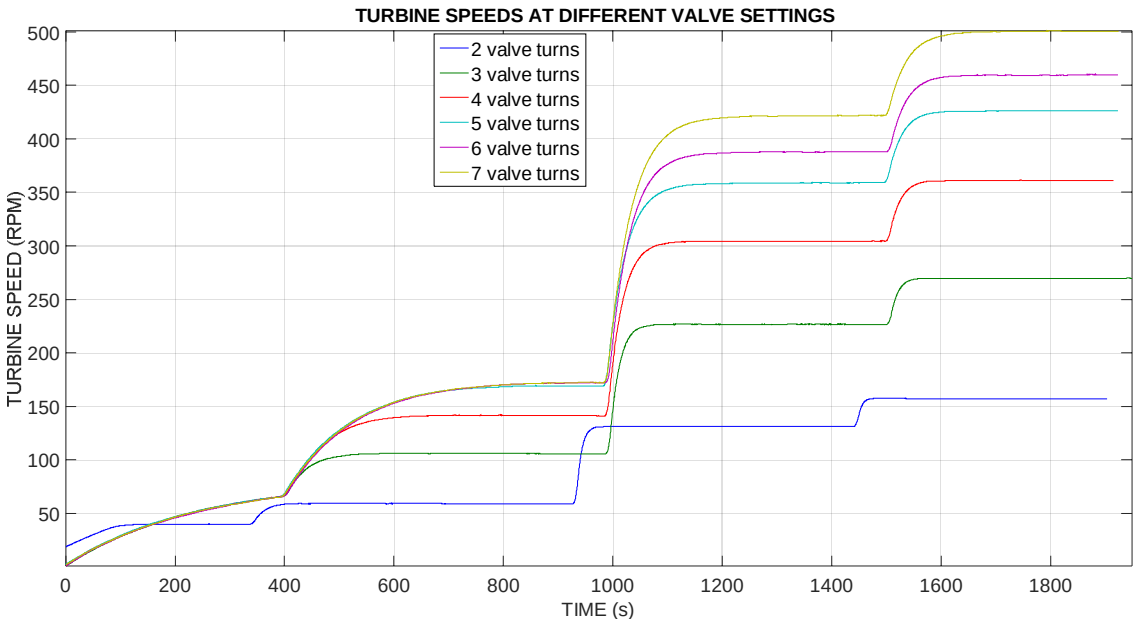

Figure 27. Rotational speed of turbine.

4.3.1 Experimental turbine torque coefficient and tip speed ratio characteristics

The torque coefficient – tip speed ratio parameter of the low inertia Savonius with augmentors (slope C) of Fig. 4 was adopted to achieve power output of commercially available wind turbine. This relationship is used to verify the adherence of the experimental turbine to the torque coefficient – tip speed ratio relationship. The similarity in the slope of the two graphs (Fig. 4 and Fig. 28) approximating to a value of 0.15 is calculated. From the maximum recoded turbine output power in the experiment, optimum tip speed ratio (see Fig. 30) is interpolated and found to be 1.2 corresponding to a torque coefficient of 0.175. Note that only the extreme valve setting (2 and 7 turns) results were repesented due to the similarity of results at different orifice setting.

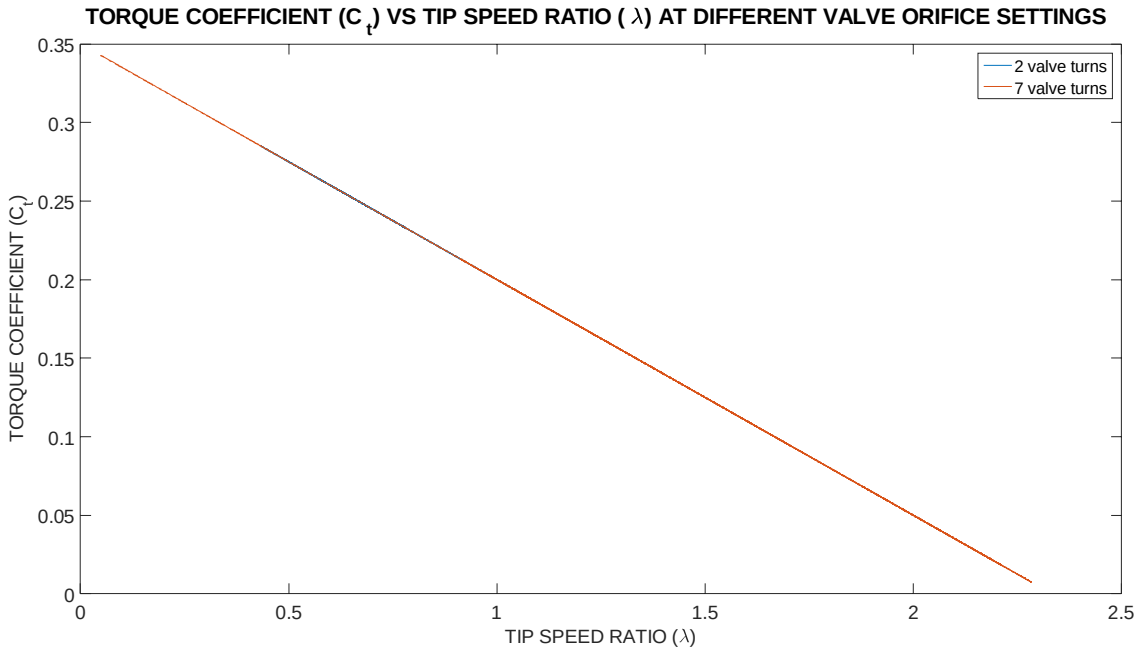

Figure 28. Torque Coefficient vs tip speed ratio for IEHEC rotor.

4.3.2 Wind Power

Change in wind power is as a result of change in wind speed and is independent of the turbine performance. Hence at maximum wind speed of 12 m/s, the power obtaiable is approximately 4.3 kW as shown in Fig. 29. As earlier noted, the deviation in result at different valve turns is consequent to off-set in data recording time. Only the extreme valve setting (2 and 7 turns) results were repesented owing to similarity in results at other valve settings.

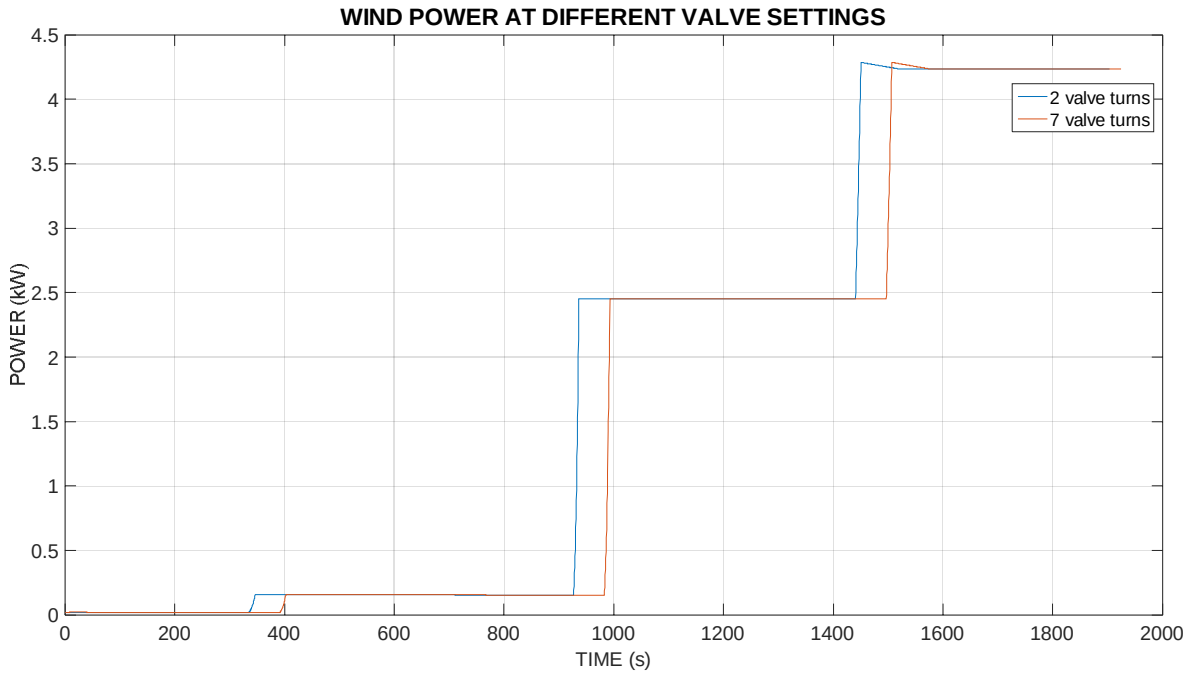

Figure 29. Wind power.

4.3.3 Turbine power output

As is earlier established, power output of the turbine is a function of the power coefficient which is dependent on the tip speed ratio of the rotor. Hence the valve orifice is adjusted so that the tip speed ratio traces the power curve of a practical turbine model. Figure 30 presents the power coefficient - tip speed ratio relationship of the experimental turbine, showing a concurrence in the power output of the turbine model in comparison to that presented in Fig.4. The optimum power coefficient of 0.205 was achieved corresponding to a tip speed ratio of about 1.2. The experimental turbine's tip speed ratio value is close to the tip speed ratio recorded in the test bench simulation (1.17) presented in Fig. 23 and the tip speed ratio in the virtual simulation (1.19) using test bench valve orifice parameter as shown in Fig. 24. Note that only results of extreme valve settings were presented following similarity in result at other valve settings.

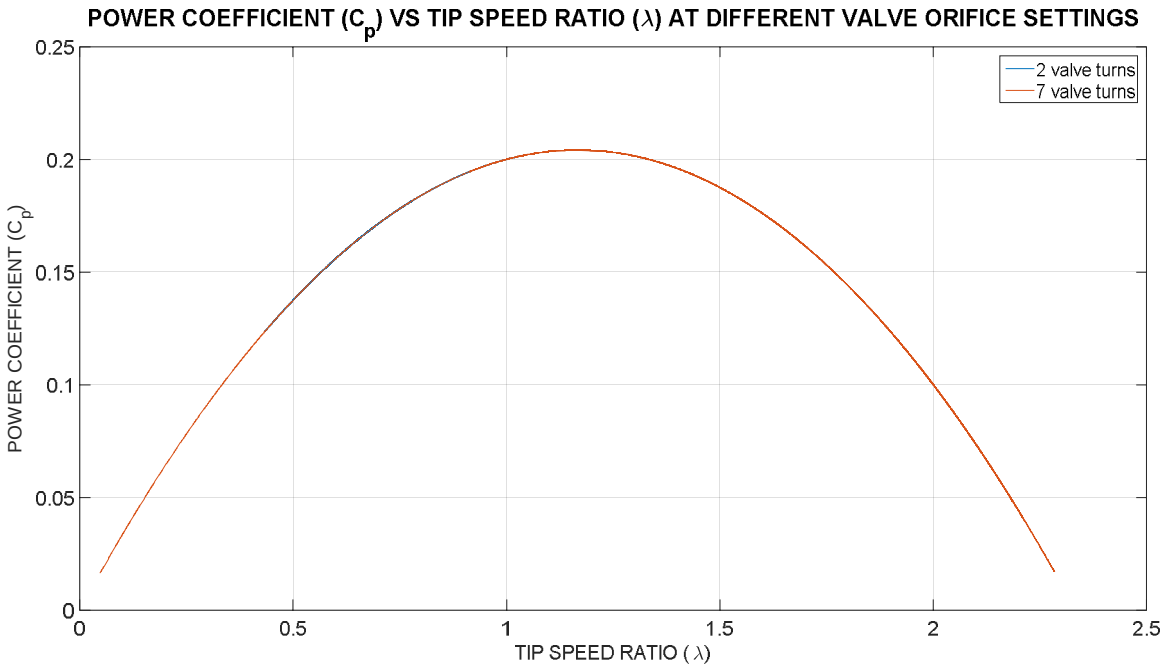

Figure 30. Power coefficient - Tip speed ratio relationship of EIHEC turbine.

4.3.4 Torque Coefficients and Tip speed ratio

Torque coefficient is defined as the ratio of power coefficient to the tip speed ratio. The optimum torque coefficient of 0.175 was achieved at 3 valve knob turns in wind speed range of 10 – 12 m/s. The optimum orifice of the test bench turbine model was calibrated in the experimental turbine. The output result is represented in Fig. 31 with the highlighted plot. The output torque coefficient observed is concurrent with the torque coefficient of the test bench presented in Fig. 25. However, the valve orifice at which the optimum parameters were achieved slightly differ in the two models; 2.5 mm (2.5 valve turns) in the virtual model and 3 mm (3 valve turns) in the experimental model. Hence the difference in the torque coefficients.

Unlike in the virtual turbine model, the optimum orifice diameter of 1.85 mm could not be realistically calibrated in the experimental set-up. Hence the orifice setting of 2.0 mm is used in the experimental turbine to evaluate the virtual turbine model parameters. Figure 32 shows the tip speed ratio of the virtual turbine model (0.65 at 2 valve turns) in comparison to the tip speed ratio of the test bench turbine (0.95 at 2.5 valve turns).

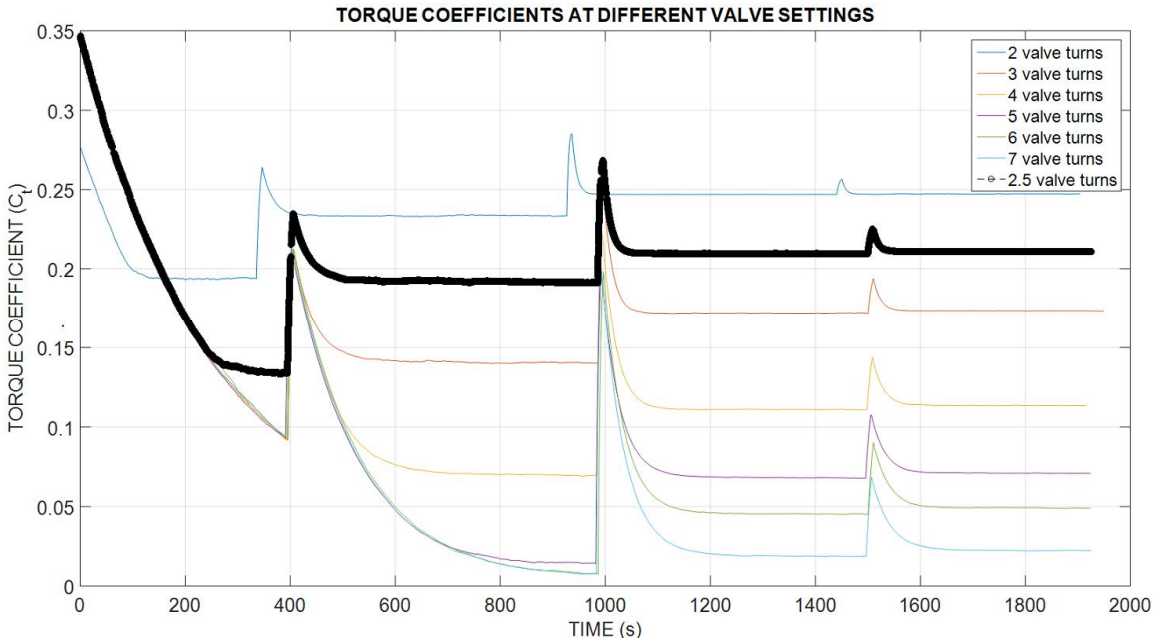

Figure 31. Torque coefficient of simulated turbine.

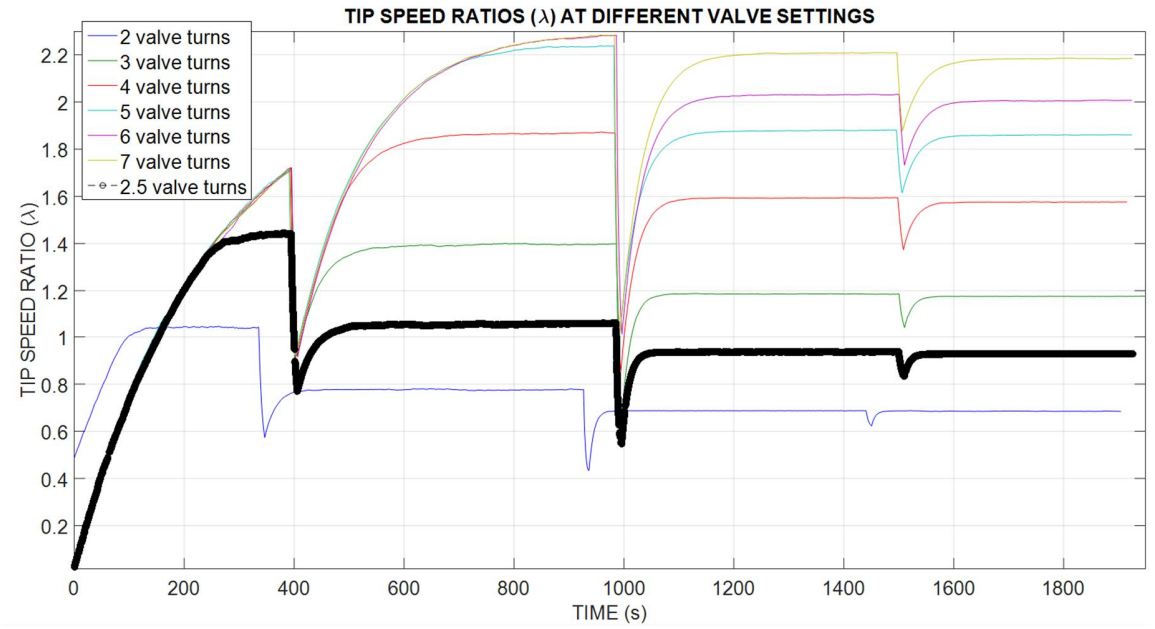

Figure 32. Tip speed ratio of turbine at different valve turns.

4.3.5 Turbine Power

Figure 33 presents output power of the turbine at different valve orifice opening and wind speed.

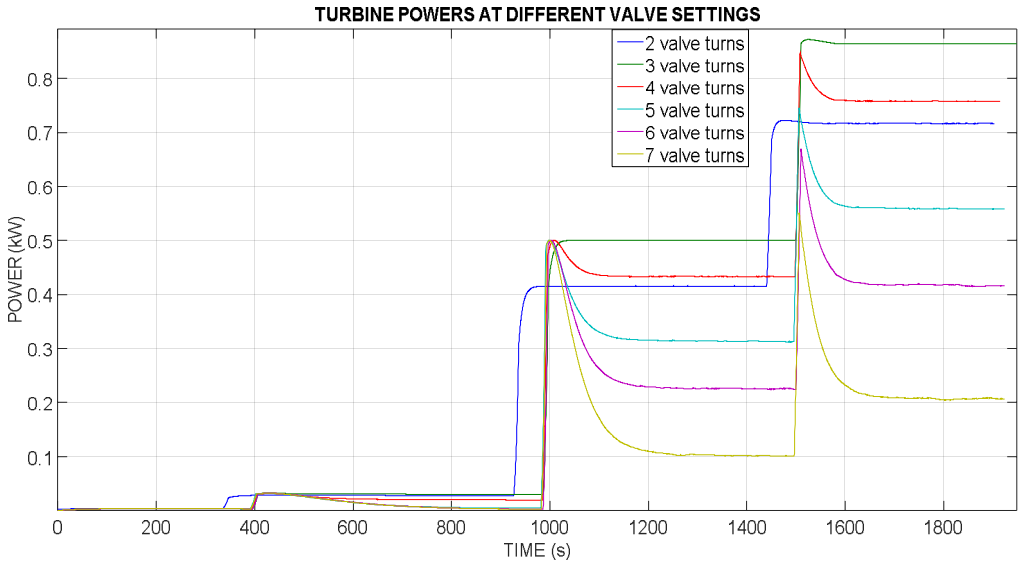

Figure 33. Turbine power.

It could be observed from the graph an increasing power output with increase in wind speed. Considerable power output is achieved between wind speeds of 10 - 12 m/s. Maximum power output was achieved at 3 turns of the valve knob. Power outputs of 0.50 kW and 0.87 kW were recorded at 10 m/s and 12 m/s wind speed respectively. In latter pages, we will evaluate the corresponding valve orifice diameter in relation to the number of turns of the valve knob.

Similarly, optimum power coefficient was recorded at 3 valve knob turns. Using the orifice area formulation, the valve orifice area was simulated. The diameter is calculated thus:

$$D = \sqrt{(4 * A_o / \pi)} \quad (23)$$

The result of Fig. 34 shows simulated valve diameter corresponding to the number of valve knob turns. The optimum valve orifice at optimum power output at 3 valve knob turns (between 10 – 12 m/s wind speed) is found to be 3 mm. The spike in the signals were as a result of disturbances in the system with changing wind speed.

The measured flow characteristic of the simulated valve closely follows the characteristic data provided by the manufacturer. This verifies the behavior of the valve in operation.

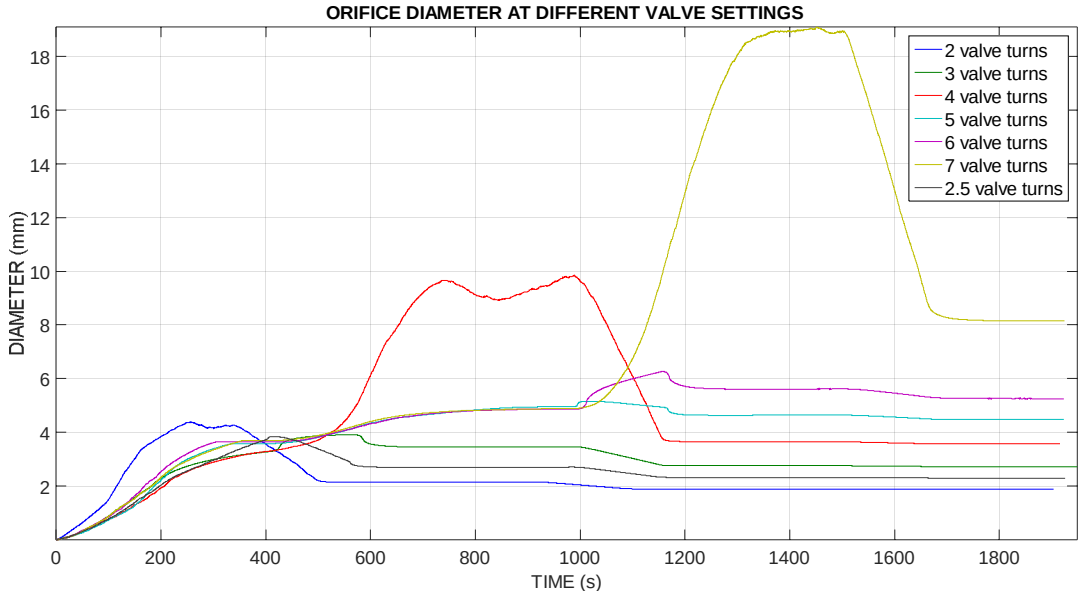

Figure 34. Valve orifice diameter.

4.3.6 Thermal Power

Thermal power (P_k) is calculated from flow and pressure drop across the valve using Eq. (16). The graph of Fig. 35 reveals the thermal power of the experimental system at different wind speed and valve orifices. Between wind speed of 2 - 4 m/s and higher number of valve turns (4 -7), an insignificant pressure difference is recorded and due to sensory limitations of the pressure transducer, negative pressure were recorded in some cases. Hence thermal power obtainable at wind speeds below 4 m/s and orifice diameter above 3 mm is insignificant with this turbine parameters. Maximum thermal power output of approximately 0.82 kW at 3 number of valve knob turns and constant wind speed of 12 m/s was achieved.

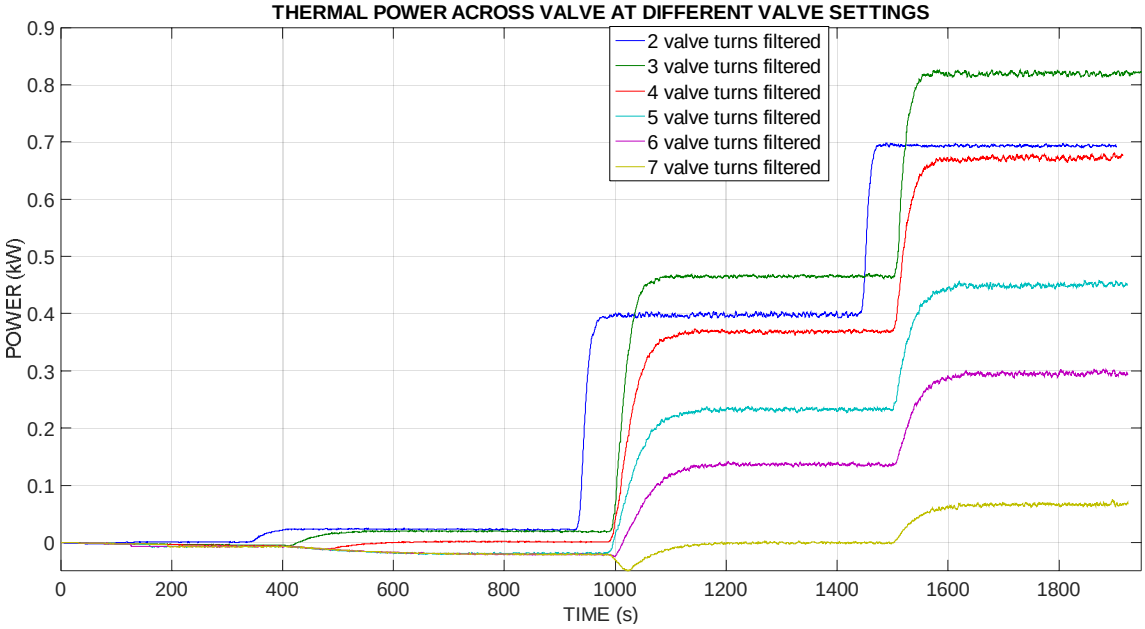

Figure 35. Thermal Power.

The power output of the system is dependent of the coefficient of performance of the system. The efficiency of the turbine in harnessing wind and the valve to generate heat were evaluated.

$$C_{pk} = \frac{P_k}{P_{wt}} \tag{24}$$

, where C_{pk} valve thermal power conversion efficiency.

From calculation, these values at wind speed of 10 m/s and 3 valve turns stand at 0.20 and 0.9 respectively. It is noticed that increasing wind speed resulted in increasing valve thermal power efficiency; an indication of high functional efficiency of chosen valve type.

Figure 36 shows power obtainable from the wind speed profile in comparison to achieved turbine power at different valve knob turns. The reference wind power is a calculation of power contained in the wind moving across the cross sectional area of the turbine blade without doing any work or obtainable at 100% power efficiency of turbine. Whereas the turbine power is calculated from power the turbine extracted from the wind at any given orifice diameter. Applying Eq. (5) and Eq. (24), the efficiency of turbine power and thermal power conversion of the system can be evaluated.

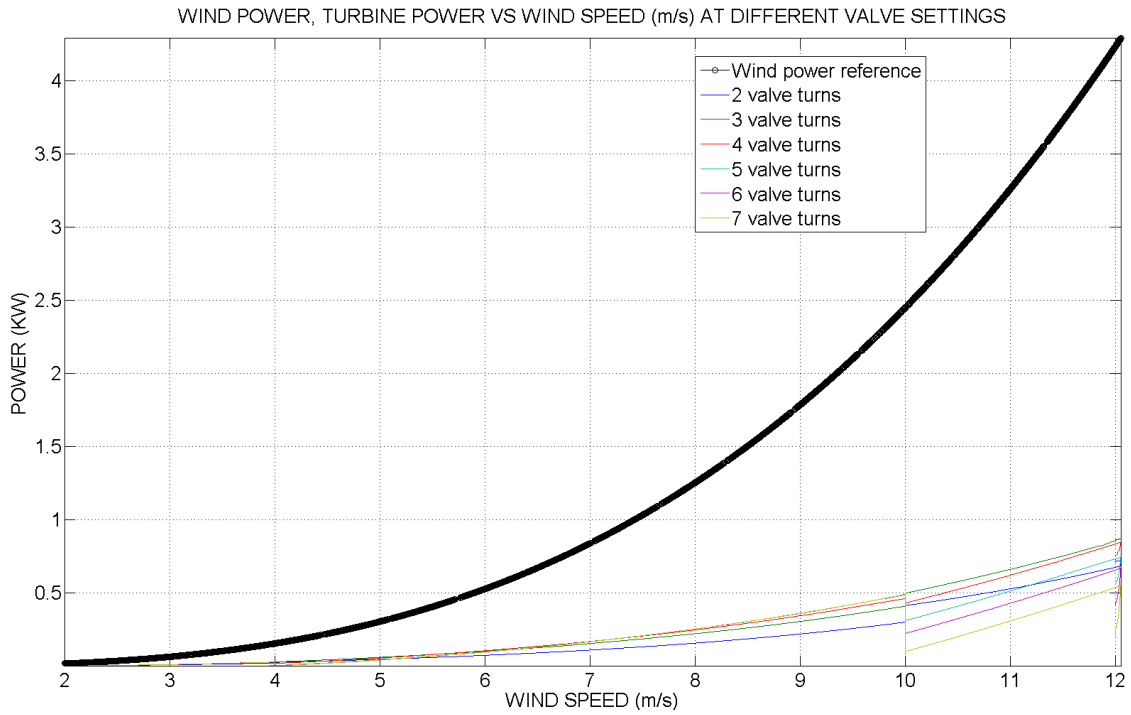

Figure 36. Turbine power in relation to wind power.

Consequent to fluid throttling is temperature rise in the fluid. Figure 37 maps the temperature change in the fluid measured at position after the throttle valve at different orifice set points. At time zero, the temperature tranceducer measures the ambient temerature of the fluid. The difference in temperature during each measurement cycle gives the heat input in the fluid. Thermodynamically, the temperature increase in the fluid resulting from pressure drop and hydraulic power required to move the mass flow across the valve orifice [35] is given by:

$$T_f - T_\infty = \frac{\Delta p}{C_{voil}\, \rho_{oil}} \tag{25}$$

At 3 mm orifice diameter setting, temperature difference of 4 ^{0}C was achieved. Noticeably, higher temperature is achieved at higher pressure build-up which corresponds to higher wind speed. It should be noted that the higher temperature recorded at 2 and 3 valve turns were as a result of difference in the innitial temperature of the oil at the start of the experiment.

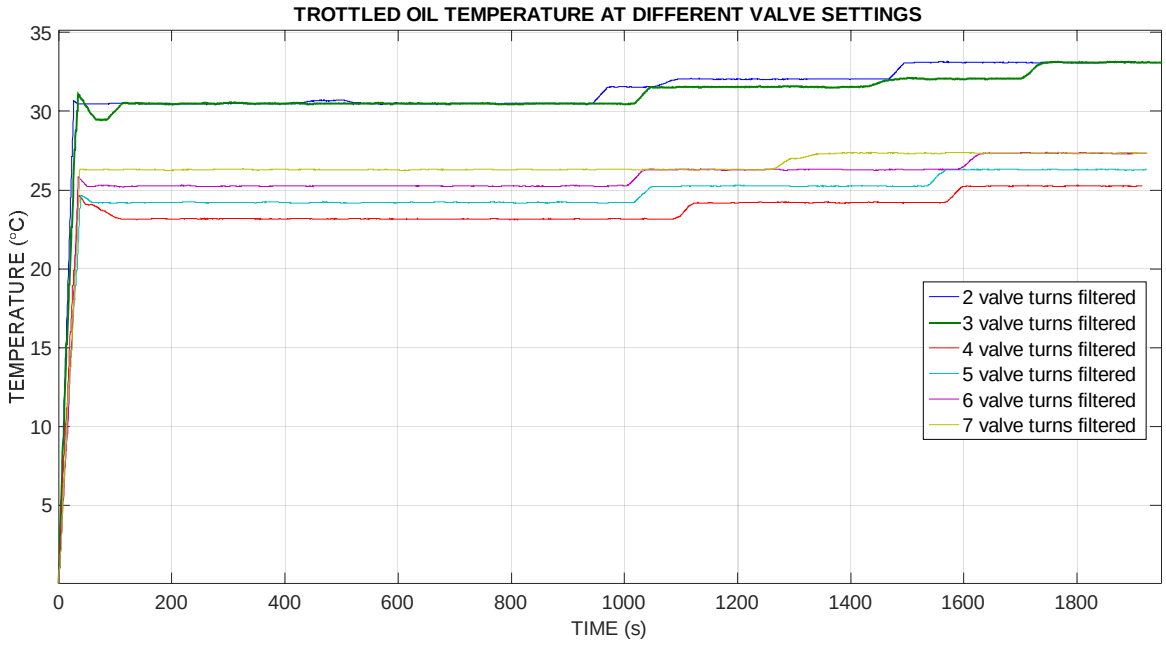

Figure 37. Throttled oil temperature.

By heat load from Eq. (18), and oil volume of 202.5 liters used in the experiment, heat load of approximately 0.8 kW was calculated. This validates the thermal power value of Fig. 35. Given an ambient air temperature of 26 °C and throttled oil temperature of 34 °C, the specific cooling capacity of the cooler could be derived by applying Eq. (20). Also it is recommended to account for deficiency due to contamination with a 10 % safety margin [40]. Hence P_{sc} = 0.1025(1.1) = 0,113 kW/^{0}C. This power loss must be dissipated by the oil cooler.

5 RECOMMENDATION

It is understood that power output by the turbine is most efficient at an optimum tip speed ratio of the turbine. In this system, the tip speed ratio and consequently thermal power output of the turbine is influenced by the orifice diameter of the valve. This parameter controls the system torque, pressure build-up and hydraulic fluid flow rate, hence a critical parameter impacting the performance of the system.

In the current model of the system, the valve in use requires manual adjustment to achieve optimum setting. Given a fixed wind speed, the valve performance will be efficient, however the dynamic wind environment requires that the valve throttle mechanism be flexible and self-adjusting to achieve optimum condition. This could be achieved by use of hydraulic proportional valve with a feedback controller.

Proportional valve suitability stems from its lower cost and maintenance requirements compared to servo valve. Using optimum tip speed ratio parameter of the turbine in closed-loop applications, the valve orifice could be adjusted with varying wind speed to operate at optimum set-point. A new semi-empirical hardware-in-the-loop simulation [45] presents a modelling approach to integrate hydraulic proportional spool valve to this hydraulic system. However considering the slow dynamics in wind turbine and heat transfer, conventional proportional vale should meet the requirement of the system.

6 CONCLUSION

The sustainability of wind energy and other renewable energy sources continues to attract investment and development in the technologies. Of known wind energy harnessing technologies, Savonius turbine has considerable low power, limiting it to small power requirements applications.

Researches on the performance of Savonius rotor under various environmental conditions and design configurations has been documented. Using a simplified augmented turbine prototype, constant wind parameter over time and varied throttle orifice diameter, the optimum operation condition of the turbine yielding maximum turbine power and system thermal power output was found. The parameters at optimum condition corresponds to orifice diameter of 3mm, tip speed ratio of 1.2 and power coefficient of 0.2. It is worth noting that no public information is made of the augmentors of the turbine prototype used. However, the power coefficient of the experimental rotor closely match the output result of Wilson *et. al* work [17]. Optimum tip speed ratio was found to slightly differ.

Other than the torque coefficient and tip speed ratio parameters of the turbine, surface area of the turbine plays into its power output. This implies that efficient design materials for the turbine need be explored to improve on the weight per unit power output of the turbine.

To maintain optimum operating condition of the system, it is recommended to substitute the throttle valve in the set-up with a solenoid actuated proportional valve to respond to the dynamic wind condition while keeping in mind the power requirement of additional control unit of the valve.

It was observed that a considerable amount of power (about 40 W) was produced at minimum wind speed of 4 m/s. The compact design of this system and potential increase in power efficiency with increased surface area of turbine makes it suitable for remote application with

high wind availability. Offshore room heating application presents a practical environment with high wind availability.

REFERENCES

[1] Herpiö, J. Simulation of Wind Powered Hydraulic Heating System [web document]. Lappeenranta: September 2014 [Referred 16.10.2015]. Master's degree thesis. Lappeenranta University of Technology, School of Energy Systems. 48 p. + appendixes 3 p. Available in PDF-file: http://www.doria.fi/bitstream/handle/10024/102229/DI-JMH20141203.pdf?sequence=2.

[2] Wortman, A. J. Introduction to Wind Turbine Engineering. National Bureau of Standards. Boston, Butterworth Publishers, 1983.

[3] Corbetta, G., Mbistrova, A. The European Offshore Wind Industry - key trends and statistics 2014. January 2015 [Referred 16.10.2015]. The European Wind Energy Association. Available in PDF-file: http://www.ewea.org/fileadmin/files/library/publications/statistics/ EWEA-European-Offshore-Statistics-2014.pdf.

[4] McCrone, A. Global Trends in Renewable Energy Investment 2015 [Referred 16.10.2015]. Frankfurt School – UNEP Collaborating Centre Frankfurt School of Finance & Management. 16 p. Available in PDF-file: http://fs-unep-centre.org/sites/default/files/attachments/key_findings.pdf.

[5] Van der Hoeven, M. Wind Energy. Technology roadmap, 2013 edition. 58 p.

[6] Wind Turbine Paper. January 2012 [Referred 16.10.2015]. AIMU Technical Services Committee. 24 p. Available in PDF-file: https://www.aimu.org/aimupapers/AIMUWindTurbinefinal7.24.pdf.

[7] Sun, Z., Tang, Z. Experimental Study on a Model of Bulk Wind Energy Collecting System. Modern Applied Science, 2011. Vol. 5, No. 2, Pp. 143-148.

[8] Menghal, P. M., Laxmi, A. J. Real Time Control of Electrical Machine and Drives: A Review. International Journal of Advances in Engineering & Technology, 2011. Vol. 1, Issue 4. Pp. 112-126.

[9] Bouscayrol, A. Hardware-in-the-loop (HIL) simulation. [Web document]. Lille: May 2009 [Referred 20.10.2015]. University of Lille1, Sciences and Technology, L2EP, France. Available in PDF-file: http://www.evs24.org/docs/EVS24hilworksop.pdf.

[10] Pat. US4114809. Wind Powered Hydraulic Heating System. (Sampson, A. R.) Appl. US 804949, 1977-9-6. Publ. 1978-19-9. 6 p.

[11] Alia, M. A. K., Younes, T. & Sarhan, H. Hydraulic Domestic Heating by Throttling. Journal of Scientific Research, 2010. Vol 2. Pp. 461- 465.

[12] Manyonge, A. W., Ochieng, R. M., Onyango, F. N. & Shichikha, J. M. Mathematical Modelling of Wind Turbine in a Wind Energy Conversion System: Power Coefficient Analysis. Applied Mathematical Sciences, 2012. Vol. 6, 2012. Pp 4527 – 4536.

[13] Ragheb, M., Ragheb, A. M. Wind Turbines Theory - The Betz Equation and Optimal Rotor Tip Speed Ratio. In: Carriveau R., editor. Fundamental and Advanced Topics in Wind Power. InTech, 2011. Pp. 19 – 38.

[14] Jones, B. Elements of Practical Aerodynamics, John Wiley and Sons, New York, United States, 1939. Pp. 8 – 41.

[15] Eldridge, F. R. Wind Machines. 2nd Edition. The MITRE Energy Resources and Environmental Series. Van Nostrand Reinhold Inc., U.S, 1980.

[16] Morshed, K. N. Experimental and Numerical Investigations on Aerodynamic Characteristics of Savonius Wind Turbine with Various Overlap Ratios [web document].

Statesboro: May 2010 [Referred 20.10.2015]. Master's degree thesis. Graduate Faculty of Georgia Southern University. 66 p. Available in PDF-file: http://digitalcommons.georgiasouthern.edu/cgi/viewcontent.cgi?article=1773&context=etd.

[17] Wilson, R. E. Lissaman, P. B. Applied Aerodynamics of Wind Power Machines. Aerovironment Inc, California, 1974.

[18] Letcher, T. Small Scale Wind Turbines Optimized for Low Wind Speeds [web document]. Published 2010 [Referred 16.10.2015]. Available in PDF-file: http://hdl.handle.net/1811/45531.

[19] Weiss, S. B. (2010) Vertical Axis Wind Turbine with Continuous Blade Angle Adjustment [web document]. Massachusetts: May 2010 [Referred 16.10.2015]. Bachelor degree thesis. Massachusetts Institute of Technology, department of Mechanical Engineering. 26 p. Available in PDF-file: http://dspace.mit.edu/bitstream/handle/1721.1/65178/745679481-MIT.pdf?sequence=2.

[20] Sathyajith, M. Wind Energy Fundamentals, Resource Analysis and Economics. Springer Berlin Heidelberg, New York, 2006.

[21] Kloeffler, R. G., Sitz, E. L. Electric energy from winds. Kansas, the College, 1946.

[22] Modi, V. J., Fernando M. S. U. K. On the Performance of the Savonius Wind Turbine. Journal of Solar Energy Engineering, 1989. Vol. III, Pp. 71-81.

[23] Kamoji, M., Kedare, S. B. and Prabhu, S. Experimental Investigations on Single Stage Modified Savonius Rotor. Applied Energy, 2009. Vol. 86, Pp. 1064-1073.

[24] Ponomarev, P. Tooth-coil permanent magnet synchronous machine design for special applications [web document]. Lappeenranta: October 2013. [Referred 16.10.2015]. Doctoral thesis. Lappeenranta University of Technology, School of Energy Systems. 111 p. Available in PDF-file: https://www.doria.fi/bitstream/handle/10024/93286/dissertation.pdf?sequence=2.

[25] Ponomarev, P., Åman, R. and Handroos, H. High Power Density Integrated Electro-hydraulic Energy Converter for Heavy Hybrid Off-highway Working Vehicles, Journal of IET Electrical Systems in Transportation, 2014. Vol. 4. Pp. 114-121.

[26] Puranen, J. Induction motor versus permanent magnet synchronous motor in motion control applications: a comparative study [web document]. Lappeenranta: December 2006. [Referred 16.10.2015]. Doctoral Thesis, Lappeenranta University of Technology, School of Energy Systems. 147 p. Available in PDF-file: https://www.doria.fi/bitstream/handle/10024/31238/TMP.objres.448.pdf.

[27] Rotation Kinematics, Moment of Inertia, and Torque [web document]. [Referred 16.10.2015]. Available in PDF-file: http://bolvan.ph.utexas.edu/~vadim/Classes/14s/linang.pdf.

[28] Fluid Power Formula web document]. [Referred 20.10.2015]. Available in PDF-file: http://hydraulicspneumatics.com/site-files/hydraulicspneumatics.com/files/archive/hydraulicspneumatics.com/Content/Site200/ebooks/01_01_2006/80281Ch22IFPBFo_00000052653.pdf.

[29] Mahmoud, N., El-Haroun, A., Wahba, E. and Nasef, M. An Experimental Study on Improvement of Savonius Rotor Performance, Alexandria Engineering Journal, 2012. Vol. 51. Pp. 19-25.

[30] Hydraulics & Pneumatics. Book 2, Chapter 18: Pressure-relief valves. [Referred 16.10.2015] Available at http://hydraulicspneumatics.com/other-technologies/book-2-chapter-18-pressure-relief-valves.

[31] Fitch, E.C., Hong, I.T. Pressure Regulation. In: Fitch, E.C, Hong, I.T., editors. Hydraulic Component Design and Selection. Oklahoma: BarDyne, Inc., 1998. Pp. 205-211.

[32] Jurić, Z., Kulenović, Z., Kulenović, D. Influence of the hydraulic relief valve poppet geometry on valve performance. In: Proceedings of the 2010 TMT 14th International Research/Expert Conference; 2010 Sep 11-18; Mediterranean Cruise. Croatia: TMT, 2010 [Referred 16.10.2015]. Pp. 517 – 520. Available in PDF-file: http://www.tmt.unze.ba/zbornik/TMT2010/005-TMT10-048.pdf.

[33] Pat. US3514074. High Energy Loss of Fluid Control. (Self, R. E.) Appl. US 599229, 1968-6-6. Publ. 1970-6-26. 12 p.

[34] Flow Control Valve. 2015. [www.flutec.com]. (Publishing place unknown): Flutec 2015. [Referred 16.10.2015]. Available: http://www.flutecvalves.com/download/pdf/DV_DVP_DVE_valves.pdf.

[35] Manring, N. D. Hydraulic control systems. John Wiley and Sons, Inc., Hoboken, New Jersey, 2005.

[36] Tullis, J. P. Hydraulics of Pipelines: Pumps, Valves, Cavitation, Transients. John Wiley & Sons, Inc., New York, 1989.

[37] Gear Type Flow meter VC. 2015. [www.krachtcorp.com]. (Publishing place unknown): Krachtcorp 2015. [Referred 16.10.2015] Available: http://www.krachtcorp.com/wp-content/uploads/2012/05/VC_USA_02-12_view.pdf.

[38] Electronic Pressure Transmitter. 2015. [www.hydac.com]. (Publishing place unknown): hydac 2015. [Referred 16.10.2015] Available: http://www.hydac.com.au/MessageForceWebsite/Sites/279/Files/HDA3800.pdf.

[39] Holman, J. P. Heat Transfer. McGraw-Hill Book Co. - Singapore, 1989.

[40] Oil/Air Cooler Units. [www. hydac.com]. (Publishing place unknown): hydac International [Referred 16.10.2015] Available: http://www.hydac.com.au/MessageForceWebsite/Sites/97/Files/e5806-1-02-05_oil-air-coolers-elc.pdf.

[41] Hydraulic Fluids Based on Mineral Oils and Related Hydrocarbons. [www.bosch.com]. (Publishing place unknown): Bosch Rexroth AG 2015. [Referred 16.10.2015] Available: http://dc-america.resource.bosch.com/media/us/products_13/product_groups_1/industrial_hydraulics_5/pdfs_4/re90220.pdf.

[42] Bartz, W. J. Synthetic Hydraulic Fluids for High Performance Applications. Proceedings of the National Conference on Fluid Power, 2000. Vol. 48. Pp. 7-20.

[43] Ultramax HVLP 46 oil. [www.valvolineeurope.com]. (Publishing place unknown): Valvoline. [Referred 16.10.2015] Available: http://www.valvolineeurope.com/english/products/hydraulic_oils/cid%289180%29/ultramax_hvlp_46.

[44] Hydraulic Fluids. [www.parker.com]. (Publishing place unknown): Parker Hannifin GmbH & Co. KG. [Referred 16.10.2015] Available: http://www.parker.com/Literature/Germany/CD_Rom%20Bauteilfreigabeliste%20Mechanik%20Hydraulik%20UK/general-fluids_UK.pdf

[45] Ferreira, J. A., Almeida, F. G. D., Quintas, M. R. Semi-empirical Model for a Hydraulic Servo-solenoid Valve. Journal of Systems and Control Engineering, 2002. Vol. 216. Pp. 237-248.

[46] Windside WS 4B / WS 4A [www.windside.com]. (Publishing place unknown): Windside [Referred 16.10.2015] Available: http://www.windside.com/filebank/141-WS-4BEng2010.pdf.

APPENDIX 1

Windside WS-4B data sheet [46].

Windside WS-4B / WS-4A:

- Weight: 800 kg (B) / 1200 kg (A)
- Swept area: 4 m2
- Generator: 50 A in delta, 28 A in star connection
- Voltage: 1-200 V in delta, 1-400 V in star connection
- WS-4B and WS-4A models max. 1000 rpm
- WS-4B stands continuous winds of 40 m/s, and WS-4A 60 m/s.

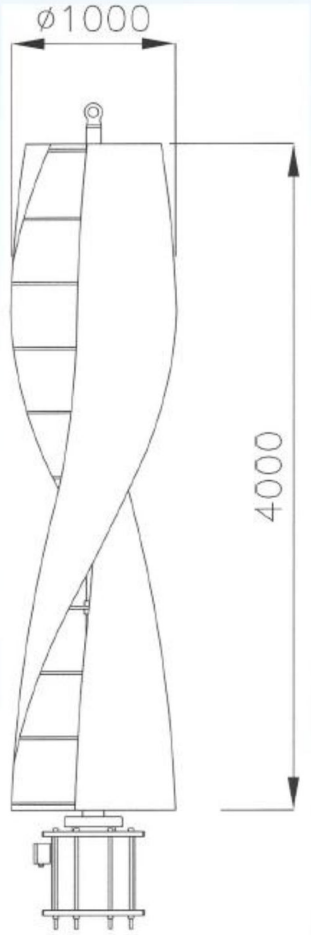

Materials:

- Vanes: fibre glass
- Fastenings: aluminium
- Generator and end plates: steel and aluminium
- All bolts stainless steel or galvanized (A4, A2 or Zn)

Assets of Windside wind turbines:

- No need to stop or secure during storms
- Produces max. amount of energy in storms
- Produces at low winds, below 3 m/s
- No need to be turned according to the wind direction
- Soundless (less than 5 dB, background noise always when measured)
- Stands snow, frost, heat, humidity and corrosion
- Allowed to be mounted on residential buildings
- Long lifespan
- Minimum need of maintenance, only lubrication

APPENDIX 2

FLUTEC NG15 Valve flow control dimensioning [34]

Model Code	Port Size	A	B	C	D	E	F	øG	øH	Weight Kg.
DV-06	1/8″	55	50	8	25	19	38	24	13	0.12
DV-08	1/4″	72	65	12.5	30	24	48	29	19	0.25
DV-10	3/8″	74	67	15	32	29	58	29	19	0.40
DV-12	1/2″	92	82	17.5	38	34	68	38	23	0.70
DV-16	3/4″	105	96	22.5	45	39	78	38	23	1.2
DV-20	1″	145	128	25	50	54	108	49	38	2.1
DV-25	1-1/4″	150	133	30	60	54	108	49	38	2.8
DV-30	1-1/2″	155	138	35	70	54	108	49	38	3.5
DV-40	2″	200	183	40	80	65	130	49	38	5.1

All Dimensions are in mm.

.

APPENDIX 3

KRACHT Flow Meter Working Characteristics [37]

Nominal size	geom. toothvolume	max. working pressure		Peak pressure		Sound pressure level	Resolution
		Standard-version	High pressure version (/79)	Standard-version	High pressure version (/79)		
	V_{gz} cm^3	p_{max} bar	p_{max} bar	$\hat{p}$ bar	$\hat{p}$ bar	L_A dB (A)	Imp/l
0.025	0.025	400	–	480	–	< 60	40 000.00
0.04	0.04	400	–	480	–	< 60	25 000.00
0.1	0.1	400	–	480	–	< 60	10 000.00
0.2	0.245	400	–	480	–	< 60	4 081.63
0.4	0.4	400	–	480	–	< 70	2 500.00
1	1.036	400	–	480	–	< 70	965.25
3	3.000	315	400	350	480	< 70	333.33
5	5.222	315	400	350	480	< 72	191.50
12	12.000	400	–	480	–	< 80	83.33
16	16.000	400	–	480	–	< 80	62.50

APPENDIX 4

HYDAC HDA 3845 pressure transducer data sheet [38]

Sensor Specifications	
Measuring ranges - bar	6, 16, 60, 100, 250, 400, 600
Overload pressure - bar	15, 32, 120, 200, 400, 800, 100
Burst pressure - bar	100, 200, 300, 500, 1000, 2000, 2000
Mechanical connection	G1/4A DIN 3852 male
Tightening torque	Approx. 15 lb-ft (20 Nm)
Parts in contact with media	Stainless steel, FPM seal
Accuracy (B.F.S.L.) including linearity, hysteresis, and repeatability	≤ ±0.15% BFSL
Temperature compensation zero point	≤ ±0.003% / °F typ. ≤ ±0.006% / °F max.
Temperature compensation over range	≤ ±0.003% / °F typ. ≤ ±0.006% / °F max.
Rise time	≤ 0.5 ms
Long-term drift	≤ ±0.1% FS typ. / year
Life expectancy	10 million load cycles (0 to 100% FS)
Weight	Approximately 180 g
Output signal	4 to 20 mA, 2 wire, $R_{Lmax} = (U_B - 10V) / 20 mA [k\Omega]$ 0 to 10 VDC, 3 wire, $R_{Lmin} = 2 k\Omega$ 0 to 20 mA, 3 wire, $R_{Lmin} = (U_B - 7V) / 20 mA [k\Omega]$
Environmental Condition	
Compensated temperature range	-13° to 185°F (-25° to 85°C)
Operating temperature range	-40° to 185°F (-40° to 85°C)
Storage temperature range	-40° to 212°F (-40° to 100°C)
Media temperature range	-40° to 212°F (-40° to 100°C)
CE mark	EN 61000-6-1 / 2 / 3 / 4
Vibration resistance to DIN EN 60068-2-6 at 10 to 500 Hz	≤ 20g
Environmental protection	IP 65
Electrical Specifications	
Supply voltage	2-wire: 10 to 30 VDC 3-wire: 12 to 30 VDC
Residual ripple suppy voltage	≤ 5%
Max supply current, 3-wire	approximately 15 mA
Reverse polarity protection of the supply voltage, excess voltage, override and short circuit protection	Standard

APPENDIX 5

HYDAC HDA 320 series ETS technical sheet [38]

Sensor Specifications	
Measuring range	-13° to 212°F (-25° to 100°C)
Rated pressure - psi	9000
Mechanical connection	G1/2 A DIN 3852 male
Tightening torque	33 lb-ft (45 Nm)
Parts in contact with media	Stainless steel, FPM seal
Accuracy	≤ ±2°F (1°C)
Temperature drift *(ambient)*	≤ ±0.0085% FS / °F max. zero point ≤ ±0.0085% / °F max. range
Weight	Approximately 300g
Output signal	4 to 20 mA, 2 wire, ohmic resistance max 400 Ω
Switching Specifications	
Type	PNP transistor
Switching current	1.2A per output
Switching cycles	≥ 100 million
Rise time to DIN EN 60751	T50 : 3s T90 : 9s
Environmental Condition	
Operating temperature range	-13° to 176°F (-25° to 80°C)
Storage temperature range	-40° to 176°F (-40° to 80°C)
Media temperature range	-40° to 212°F (-40° to 100°C)
CE mark	EN 61000-6-1 / 2 / 3 / 4
Vibration resistance to DIN EN 60068-2-6 at 0 to 500 Hz	≤ 10g
Environmental protection	IP 65
Electrical Specifications	
Supply voltage	20 to 32 VDC
Residual ripple suppy voltage	≤ 5%
Current consumption	100 mA *(plus switching current)*
Reverse polarity protection of the supply voltage, excess voltage, override and short circuit protection	Standard
Display	7 segment LED display, 3 digits